Blusztajn et al. (2026)
Thallium isotopic constraints on the genesis of heterogeneous mantle plume source in Taha'a (Society Islands): Implications for temporal evolution of ocean island basalts
Advances in Geochemistry and Cosmochemistry 2(1): 963, https://doi.org/10.33063/agc.v2i1.963

Research article

Thallium isotopic constraints on the genesis of heterogeneous mantle plume source in Taha'a (Society Islands): Implications for temporal evolution of ocean island basalts

Jerzy Blusztajn[1]✉ Sune G. Nielsen[1,2] George Segee-Wright[2] Ann G. Dunlea[3] Veronique Le Roux[1,2]

[1] Department of Geology and Geophysics, Woods Hole Oceanographic Institution, 02543 Woods Hole, MA, USA
[2] Centre de Recherches Pétrographiques et Géochimiques, CNRS, University of Lorraine, 15 rue Notre Dame des Pauvres, 54500 Vandoeuvre-lès-Nancy, France
[3] Department of Marine Chemistry and Geochemistry, Woods Hole Oceanographic Institution, 02543 Woods Hole, MA, USA

✉ **Correspondence to:** Jerzy Blusztajn: jblusztajn@whoi.edu

Author contributions: Conceptualization: JB, SGN, VLR; Formal analysis: JB; Funding acquisition: SGN; Investigation: JB; Methodology: JB, SGN, VLR, AGD; Supervision: SGN; Writing – original draft: JB; Writing – review & editing: JB, SGN, VLR, AGD, GSW

Data, code, and outputs: Blusztajn et al. (2026): https://doi.org/10.60520/IEDA/114421

Submitted: 2025-08-18
Accepted: 2026-02-17
Published: 2026-05-06

Production editor:
Ananya Mallik

Handling editor:
Abigail Barker

Reviews:
Nicole Williamson,
Julie Prytulak

Copyediting:
Anselm Loges,
Marthe Klöcking

Mantle plumes are chemically and lithologically heterogeneous, as reflected by the range of compositions observed in ocean island basalts (OIB). Some plume-derived volcanics may also record compositional differences between the main volcano-building (shield) stage and post-erosional volcanism. Although these temporal variations have generally been attributed to a shift in the nature of the source, variations in its chemical and lithological components remain debated. Here we present new thallium (Tl) isotope measurements in OIB lavas from Taha'a in the Society Islands, along with major elements, radiogenic isotopes and trace element ratios. We show that older (3.4–2.6 Ma) shield lavas exhibit correlations between radiogenic Sr and Pb isotope values, Nb anomalies, Ce/Pb, and Tl isotopic compositions. These correlations are consistent with recycled continentally derived sediment in most shield stage lavas with a lesser influence from subduction-modified old altered oceanic crust (AOC). In comparison, young (1.4–1.1 Ma) post-erosional lavas are characterized by unradiogenic Sr and Pb isotopes, positive Nb anomalies, and very light Tl isotopes. The mantle source of these lavas carries "young HIMU" (i.e. high U/Pb that has resided < 1 billion years in the mantle) characteristics and can be explained by recycling of subduction modified AOC in the mantle source with a relatively short residence time in the mantle prior to plume eruption at the surface.

1 Introduction

Material recycling through subduction and delamination contributes to mantle heterogeneity (e.g., Zindler and Hart, 1986; Hofmann, 1997; Stracke et al., 2003). Different isotopic systems provide abundant evidence that sediments and altered oceanic crust (AOC) are transported with the subducting plate and stored or convectively dispersed in the upper mantle, giving rise to a variety of mantle compositional endmembers (e.g., Hart, 1988; Stracke et al., 2005). Plumes and associated hotspot volcanism provide a window into the variability in mantle composition. They are often chemically and lithologically heterogeneous, containing both depleted and enriched components (e.g., White, 2010, and references therein).

In addition, the evolution of hotspot volcanism often progresses in a specific sequence. In the classic case of Hawai'i, the first volumetrically small stage is called pre-shield volcanism, followed by the main shield stage, during which 95–98 % of the volume of the volcano is erupted (Clague and Dalrymple, 1987). After a 0.5–2 Myr hiatus, the final stage is the post-erosional or rejuvenated stage, which typically comprises less than 1 % of total volcanism and is characterized by eruptions of highly alkalic basalts with distinct isotopic signatures (Garcia et al., 2010). Although not all hotspot islands show post-erosional volcanism, it has been described in several other ocean islands such as

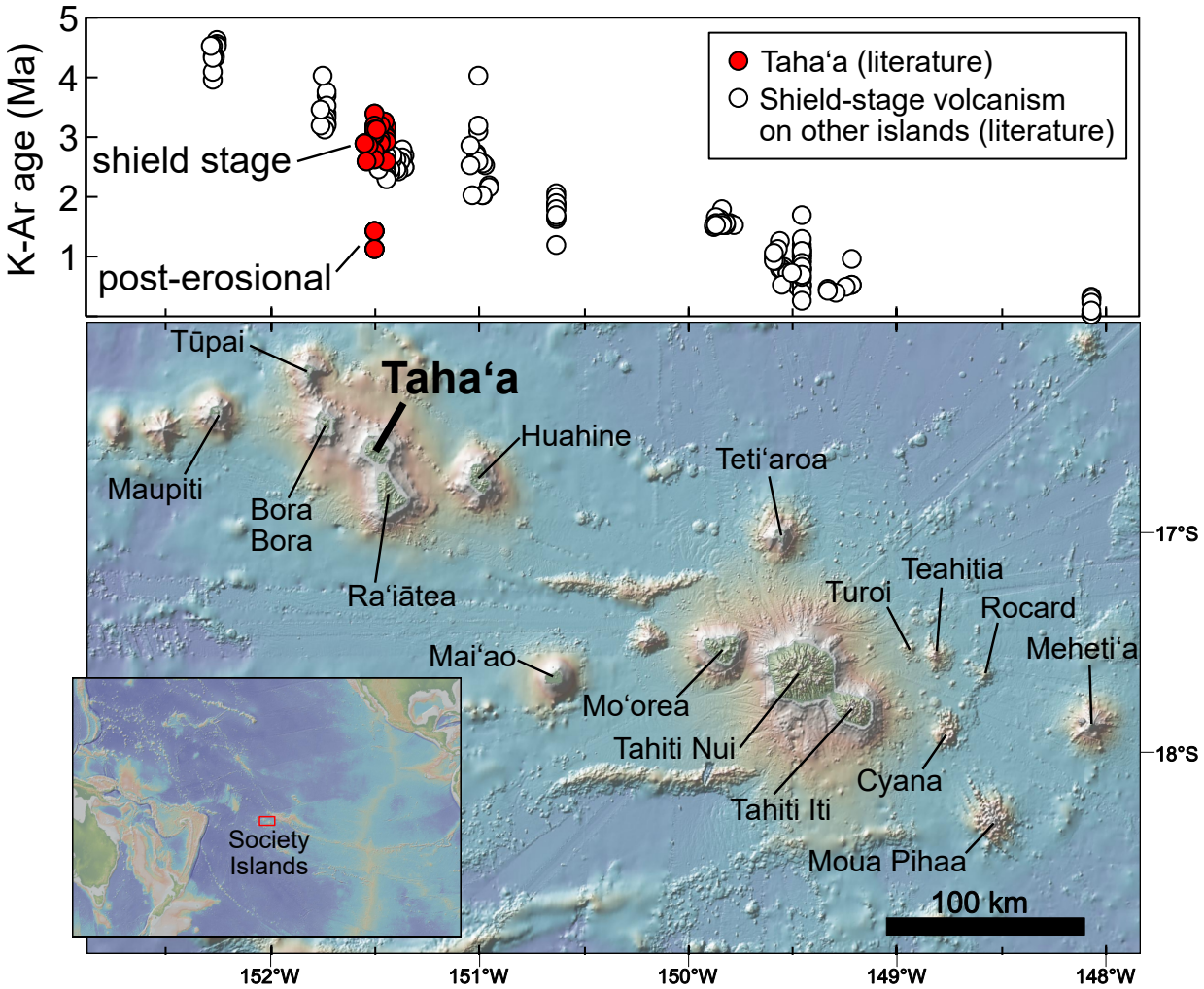

Figure 1. Map of the Society Islands. Samples from this study are from Taha'a, which is labelled in bold. An inset map shows the location of the Society Islands in the southwest Pacific. Above the map is a plot of K-Ar eruption ages of basalts from the Society Islands vs longitude (same as longitude axis of the map). Shield stage volcanism in the Society Islands follows a clear age progression with the youngest samples in the southeast. Taha'a shield stage basalts fall along this age progression, but Taha'a post-erosional samples fall off this age progression. Error on K-Ar ages ranges from 0.002–0.31 Ma. K-Ar data are from Duncan and McDougall (1976), Binard et al. (1993), Duncan et al. (1994), White and Duncan (1996), and Uto et al. (2007). Figure made with GeoMapApp (www.geomapapp.org).

the Society Islands (White and Duncan, 1996), Canaries (Hoernle and Schmincke, 1993), Samoa (Konter and Jackson, 2012), Madeira (Geldmacher and Hoernle, 2000) and Mauritius (Paul et al., 2005). Previous work has explained these temporal variations as the result of changes in mixing proportions between plume components and ambient mantle, heterogeneous plume compositions with time (e.g., White and Duncan, 1996; Konter and Jackson, 2012; DeFelice et al., 2019; Harrison et al., 2020; Cordier et al., 2021), or exhaustion of the most fertile material within the plume (e.g., pyroxenites) leading to low degree melting of the residual peridotitic mantle during late lateral spreading of the plume (White, 2010, and references therein).

In this study, we investigate the evolution of volcanism on the island of Taha'a, a small island that belongs to the Society Islands volcanic chain in French Polynesia (Fig. 1). The Society Islands consists of several islands, atolls, and seamounts stretching across 700 km that were erupted onto ~60 Ma oceanic lithosphere (Duncan et al., 1994) and following an age progression from 4.6 Ma volcanism in the northwest to < 0.5 Ma volcanism in the southeast tracking the Society plume (Fig. 1; e.g., White and Duncan, 1996; Uto et al., 2007; Cordier et al., 2021). Taha'a is located to the northwest leeward end of the Society Islands (Fig. 1). Volcanic activity at Taha'a took place in two stages, the first main shield phase between 3.4 Ma and 2.6 Ma and the second post-erosional between 1.4 Ma and 1.1 Ma (White and Duncan, 1996, Fig. 1). The Society Islands have classically been considered an EM2 mantle endmember (e.g., Hart, 1988, Fig. 2), which is thought to represent subducted sediment (e.g., White and Hofmann, 1982; Jackson et al., 2007). However, it remains uncertain whether the EM2 endmember at Taha'a contains mixtures of different sedimentary types (pelagic and terrigenous), and whether its composition evolved throughout different stages of volcanism either due to upwelling of a new component within the plume or exhaustion of the most fertile components during the main shield stage. The motivation

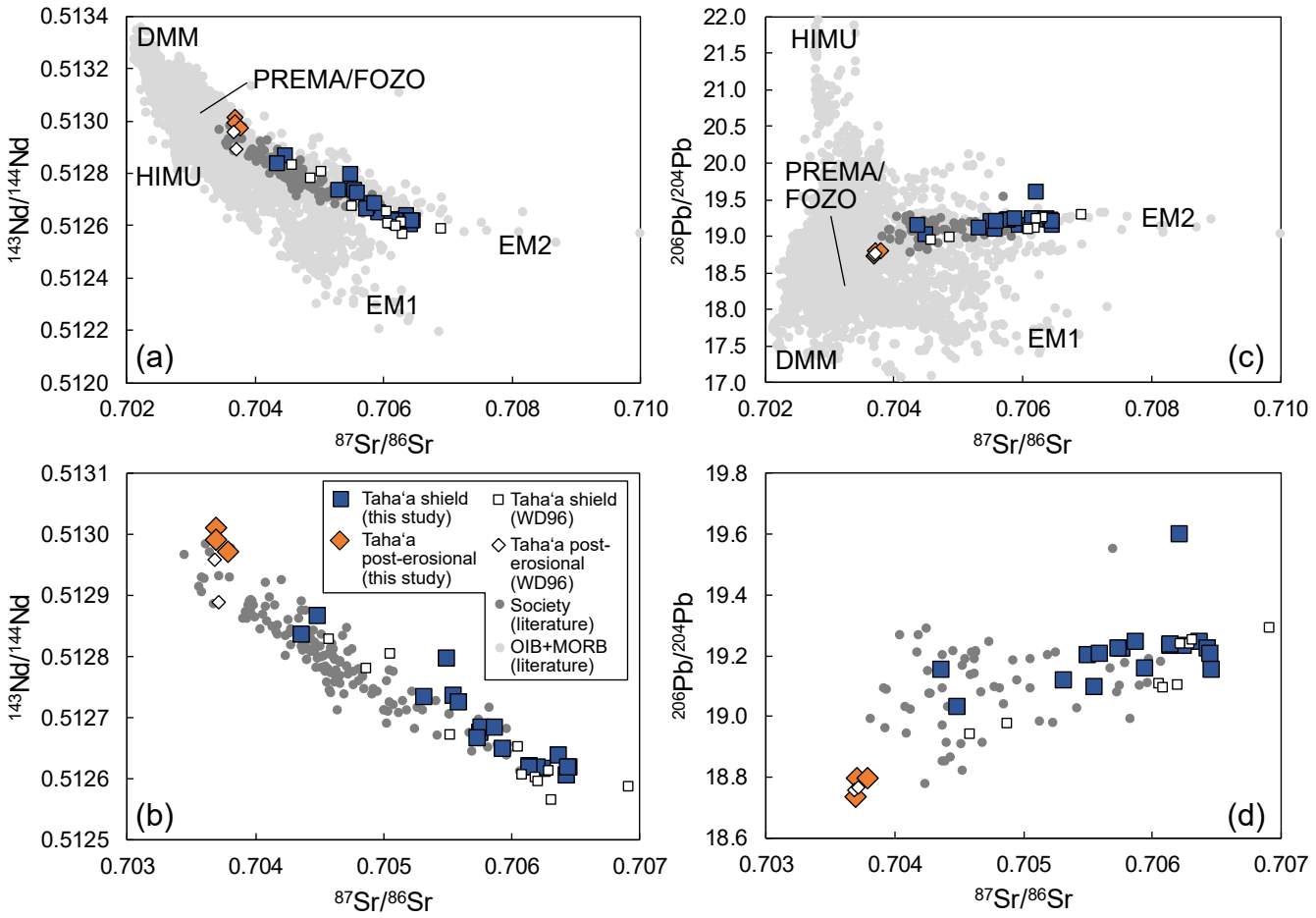

Figure 2. Radiogenic isotope bivariate plots. (a–b) $^{87}Sr/^{86}Sr$ versus $^{143}Nd/^{144}Nd$ and (c–d) $^{87}Sr/^{86}Sr$ versus $^{206}Pb/^{204}Pb$. (a, c) Compiled Society Island samples (dark grey symbols; Harðardóttir and Jackson, 2025), Taha'a samples from this study (colored symbols), and Taha'a samples from White and Duncan (1996, WD96; open symbols) are compared to a global compilation of ocean island basalts (OIB) and mid-ocean ridge basalts (MORB) from Stracke (2012) and Harðardóttir and Jackson (2025). Mantle compositional endmembers are labelled in (a) and (c) based on Weis et al. (2023). (b, d) Comparison of samples analyzed in this study with samples from Taha'a which were dated and classified by White and Duncan (1996) as representing young post-erosional and old shield stage (open diamonds and squares, respectively). Results from this study denoted as post-erosional (orange, filled diamonds) and shield stage (blue, filled squares). Taha'a samples span the entire range of radiogenic isotope compositions measured in Society Islands basalts (dark grey symbols). Measurement errors are all smaller than data point symbols.

for this work is to address these questions and determine the origin of the previously observed temporal compositional change from the main shield stage to the rejuvenated phase of volcanism.

Thallium (Tl) isotope ratios ($\varepsilon^{205}Tl$), have emerged as a complementary tool to radiogenic isotopes for studying crustal recycling processes (e.g., Nielsen et al., 2006a; Blusztajn et al., 2018; Brett et al., 2021; Williamson et al., 2021). The Tl isotope compositions of modern oxic Fe-Mn pelagic sediments (up to $\varepsilon^{205}Tl = +15$; Rehkämper et al., 2002, 2004) and oceanic crust altered at low temperatures ($\varepsilon^{205}Tl = -2$ to -15; Nielsen et al., 2006b) deviate significantly from the modern mantle ($\varepsilon^{205}Tl = -2 \pm 1$; Nielsen et al., 2006b). Furthermore, substantial Tl transport by fluids from the subducting slabs (Noll et al., 1996; Nielsen et al., 2017a) is not associated with detectable Tl isotope fractionation (Shu et al., 2019, 2022a), and so dehydrated subducted material in the deep mantle will preserve Tl isotope compositions inherited from their protoliths. Lastly, there is a large contrast in concentrations between Tl-rich recycled lithologies (~0.5–250 ng/g in low-T AOC; ~20–180 µg/g in Fe-Mn sediments; Rehkämper et al., 2002; Nielsen et al., 2006b) and Tl-poor depleted mantle (~0.5 ng/g; Nielsen et al., 2014), even when significant amounts of Tl are cycled back to the surface in subduction zones (Shu et al., 2022a,b; Nielsen et al., 2017a; Blusztajn et al., 2018). Therefore, only a very small percentage of recycled subducted components (sediments and AOC) is required to significantly modify the thallium isotopic signature of mantle-derived melts, making Tl isotopes an excellent tool to distinguish different sources of heterogeneity in the mantle.

Here we show that the compositional change in the Taha'a mantle plume from the shield stage to the post-erosional stage corresponds to a substantial negative shift in Tl iso-

tope compositions that is accompanied by changes in trace element ratios and radiogenic isotopes. These observations imply that AOC became the dominant component of the mantle plume during the post-erosional stage of volcanism.

2 Analytical methods

2.1 Sample preparation

All samples analyzed in this study were collected by Erik Hauri in 1990. Samples were crushed into 2–5 mm fragments, which were then cleaned in 18.2 MΩ-grade water. Rock chips without visible signs of alteration were carefully handpicked under a binocular microscope. 200–300 mg of such material was dissolved for Tl isotope and trace element measurements in a 3:1 mixture of concentrated HF+HNO_3 on a hotplate at 100 °C for at least 24 hours. Samples were ultrasonicated to ensure that fluorides formed at the rock chip surfaces did not prevent reaction between silicate and HF. Once the rock chips were fully dissolved with only a white fluoride powder remaining, the samples were dried down and fluxed several times with concentrated nitric acid and hydrochloric acid until the fluorides that formed during dissolution could no longer be seen.

In order to check if any isotopically anomalous Tl was present in secondary alteration minerals in the separated rock chips, separate aliquots of rock chips for five samples, which cover the total variations observed in unleached samples were also leached in 1 mol/L HNO_3 before the standard HF-HNO_3 dissolution performed for all the samples. Acid leaching (using HCl or HNO_3) of lavas has previously been shown to be important for submarine lavas in which either seawater alteration or deposition of Mn oxides can substantially modify the bulk Tl isotope composition (Nielsen et al., 2016; Williamson et al., 2021). The acid leaching efficiently removes these secondary minerals, leaving only Tl associated with the lava behind (Nielsen et al., 2016). Although subaerial weathering of both basaltic and felsic rock types appears to be associated with no detectable Tl isotope fractionation (Nielsen et al., 2005), it is unknown if such processes could cause addition of isotopically anomalous Tl. Thus, we only investigated a subset of the samples to confirm the absence of such effects. Five samples were leached in 1 mol/L HNO_3 for one hour in an ultrasonic bath followed by 3 times rinse in 18.2 MΩ-grade water. Although previous Tl isotope work has primarily used HCl to leach lavas (Nielsen et al., 2016; Williamson et al., 2021; Kaare-Rasmussen et al., 2025), leaching procedures using HNO_3 are common for sediments and show that Mn oxides are also soluble in this media (Wang et al., 2022). Secondary clay minerals are unlikely to fully dissolve in HCl or HNO_3 because they are silicates. However, ultrasonication in strong mineral acids effectively removes these secondary minerals from sample surfaces and renders residual chips of lava free from contamination (Nielsen et al., 2016). The residual rock chips were then dissolved following the same procedure as the unleached samples.

2.2 Thallium isotope measurements

Chemical separation of Tl was performed following methods described in Nielsen et al. (2004) using two-stage anion exchange chromatography. Thallium isotopic compositions were measured using a Thermo Neptune multicollector-inductively coupled plasma mass spectrometer (MC-ICP-MS) located in the Plasma Facility at Woods Hole Oceanographic Institution (WHOI). Measurement protocols were based on previously described techniques that utilize NIST SRM 981 Pb added to all samples for external mass bias correction and NIST SRM 997 Tl for standard-sample bracketing (Nielsen et al., 2004). The Tl isotope compositions are reported relative to NIST SRM 997 Tl in parts per 10 000:

$$\varepsilon^{205}\mathrm{Tl} = 10\,000 \times \frac{\left(^{205}\mathrm{Tl}/^{203}\mathrm{Tl}_{\mathrm{sample}} - {}^{205}\mathrm{Tl}/^{203}\mathrm{Tl}_{\mathrm{SRM\,997}}\right)}{\left(^{205}\mathrm{Tl}/^{203}\mathrm{Tl}_{\mathrm{SRM\,997}}\right)}$$

Total procedural blanks throughout this study were ~2 pg, which is insignificant in comparison to the lowest analyzed Tl content of 5 ng. Each sample solution was analyzed twice with repeatability of ± 0.1–0.3 ε^{205}Tl. The uncertainty of the Tl isotope measurements, which is applied throughout in this manuscript is estimated to be around 0.5 ε^{205}Tl-units based on repeat measurements of the USGS BHVO-1 reference material analyzed together with samples ($\varepsilon^{205}\mathrm{Tl} = -3.6 \pm 0.5$; 2σ, n = 5) that agrees well with the literature value of $\varepsilon^{205}\mathrm{Tl} = -3.5 \pm 0.5$ (e.g., Nielsen et al., 2016; Shu et al., 2017, 2019).

2.3 Radiogenic isotope measurements

Sr, Nd, and Pb isotopic analyses were implemented using 50–100 mg of rock chips leached for 1 hour in warm 6.2 mol/L HCl and then dissolved following a similar procedure as dissolutions for Tl isotopes. Sr and Nd separation was performed using Sr-Spec and Ln-Spec resin, respectively, following previously published procedures (e.g., De Muynck et al., 2009; Scher and Delaney, 2010). Lead was separated following the HBr-HNO_3 procedure of Abouchami et al. (1999) using a single column pass. Isotope compositions of Sr, Nd, and Pb were performed on the Neptune MC-ICPMS at the WHOI Plasma Facility. For Sr and Nd, the internal precision is 10–20 ppm (2se); external precision, after normalization to 0.710240 and 0.512104 for the SRM 987 and JNd-1 Nd standards, respectively, is estimated to be 15–25 ppm (2se). The precision of the reported Pb isotope ratios is between 50 and 200 ppm for $^{206}Pb/^{204}Pb$, $^{207}Pb/^{204}Pb$, $^{208}Pb/^{204}Pb$, whereas external reproducibility on runs of NIST SRM 981 is better than 400 ppm (2se) for $^{206}Pb/^{204}Pb$, $^{207}Pb/^{204}Pb$, and $^{208}Pb/^{204}Pb$. Pb isotope ratios are normalized to the SRM 981 values of Todt et al. (1996). Repeated measurements of standards yielded the following mean values: $^{87}Sr/^{86}Sr = 0.710296 \pm 0.000004$ (2se; n = 4) for NBS SRM 987, $^{143}Nd/^{144}Nd = 0.512079 \pm 0.000004$ (2se; n = 4) for JNdi-1, and $^{206}Pb/^{204}Pb$=16.9379 ± 0.0007, $^{207}Pb/^{204}Pb = 15.4879 \pm 0.0002$, $^{208}Pb/^{204}Pb = 36.6907 \pm 0.0007$ (2se; n = 5) for NBS SRM 981. The USGS reference material BHVO-1 was measured

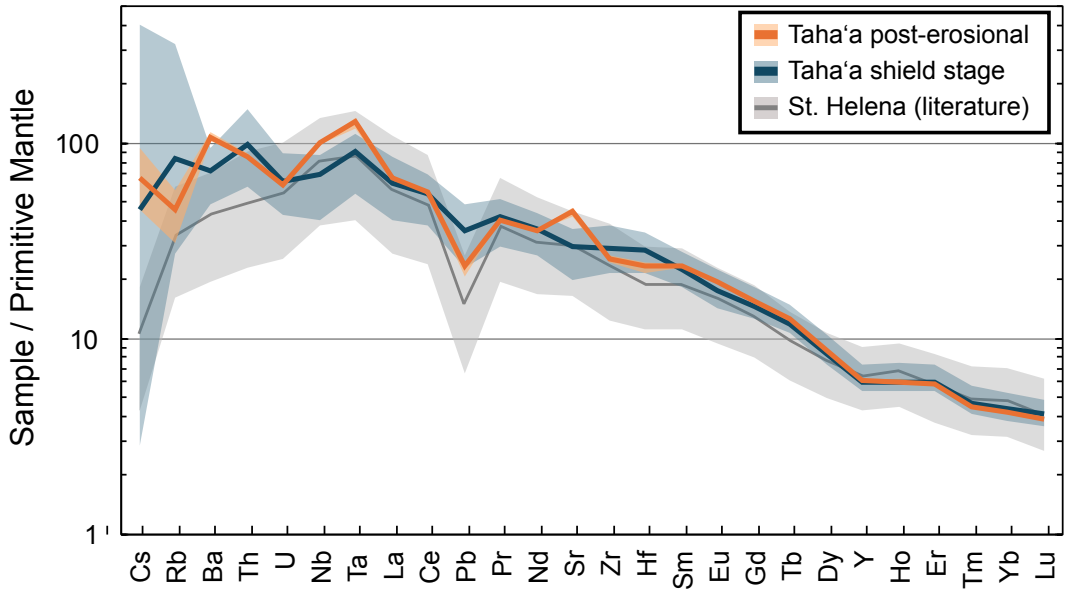

Figure 3. Primitive mantle (McDonough and Sun, 1995) normalized average trace element abundances in shield stage and post-erosional stage lavas. HIMU basalts from St. Helena (gray line) are shown for comparison (Willbold and Stracke, 2006). Population average values are shown with the bold lines and the total range is shown by the shaded areas.

as unknown. Its results for Sr, Nd, and Pb were $^{87}Sr/^{86}Sr = 0.703466 \pm 0.000010$ (2se), $^{143}Nd/^{144}Nd = 0.512980 \pm 0.000020$ (2se), $^{206}Pb/^{204}Pb = 18.694 \pm 0.00012$ (2se), $^{207}Pb/^{204}Pb = 15.574 \pm 0.00020$ (2se), and $^{208}Pb/^{204}Pb = 38.361 \pm 0.00060$ (2se), which are within error of published values (Weis et al., 2006).

2.4 Major and trace element concentration measurements

Major element concentrations (SiO_2, Al_2O_3, Fe_2O_3, MgO, CaO, MnO, Na_2O, K_2O, TiO_2, P_2O_5) were determined using the Agilent 5900 ICP-OES system in the WHOI Plasma Facility. 100–290 mg of sample powder was mixed with 400 mg of lithium metaborate ($LiBO_2$) and 40 µL of LiBr solution in platinum crucibles and heated at 1000 °C for 10 min in a Katanax X-300 fluxer. The resulting molten mixture was poured into 100 mL of 10 % nitric acid and stirred with a clean stirbar. Once completely dissolved, 3 mL of the solution was further diluted with 9 mL of 10 % nitric acid (12 mL total) before being analyzed. Concentrations were quantified by constructing calibration curves with USGS rock reference materials BHVO-1, AGV-2, and BCR-1. The USGS reference material BIR-1 was also analyzed and treated as an unknown together with samples. The measured major element concentrations for this standard agree well with recommended values (Jochum et al., 2016) within 5 %, except K_2O which is 9 wt.% off from the accepted value. Elemental concentrations were converted to oxide form and totals were calculated to ascertain that the entire sample had been accounted for in the analyses. A few samples returned totals higher than 100 % (up to 12 % higher), which we ascribe to changes in instrument drift that were unaccounted for because no internal standard was added during the ICP-OES measurements. In order to correct for this drift, we normalized all major element oxide totals to 100 %.

Trace element concentrations were measured using a Thermo Electron iCAP-Q ICPMS located in the Plasma Facility at WHOI. Calibration curves were generated based on rock reference materials AGV-1, BCR-1 and BIR-1 using the concentrations from the compilation by Jochum et al. (2016) as true values. Instrument drift was monitored and corrected via normalization to indium intensities. BHVO-1 reference material was measured as an unknown to check the measurement accuracy. These produced values within 7 % of the compiled best estimates (Jochum et al., 2016), which is consistent with the long-term uncertainty typically observe in data published from the Plasma Facility at WHOI (e.g., Shu et al., 2017, 2019). Exceptions were the elements Ho, Ta, Pb, Th, and U that exhibited deviations of 12 %, 12 %, 14 %, 17 %, and 13 % from the literature values, respectively.

3 Results and Discussion

3.1 Geochemistry of Taha'a shield and post-erosional lavas

White and Duncan (1996) used K-Ar dating to show that Taha'a lavas fall into two stages of volcanism: shield (3.4–2.6 Ma) and post-erosional (1.4–1.1 Ma). They showed that the radiogenic isotope and trace element signatures for these stages are significantly different, with $^{87}Sr/^{86}Sr = 0.7046$–0.7069 for shield-stage samples and $^{87}Sr/^{86}Sr = 0.7036$–0.7037 for post-erosional samples (Fig. 2b,d). Samples from this study span similar ranges of radiogenic isotope (see Table 3) and trace element (see Table 2) compositions and so can be divided in shield stage (n = 19) and post-erosional (n = 3) samples based on these similarities to lavas from White and Duncan (1996). It is worthwhile to emphasize

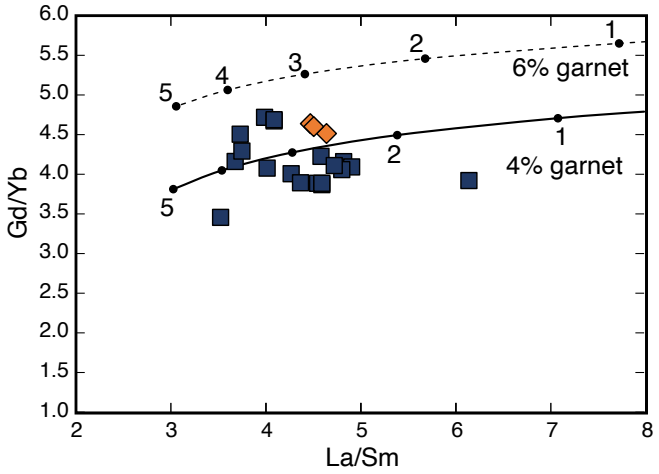

Figure 4. Gd/Yb vs La/Yb diagram for Taha'a lavas plotted together with melt curves obtained using accumulated fractional partial melting of garnet lherzolite of primitive mantle source composition (McDonough and Sun, 1995). Two curves labelled garnet 4 % and 6 % represent the abundance of garnet in the source with tick marks indicating the degree of melting in %. Partition coefficients reported in Krein et al. (2020) are used in the calculation. Symbols as in Figure 2.

that isotopic variations within a single island of Taha'a are approximately equal to variations of the whole Society Island volcanic chain (Fig. 2d).

Both the shield stage and post-erosional samples are alkalic and range from tephrite basanites to alkali basalts in composition with limited variations of MgO from 7.7–12.2 wt.% (see Table 1). The primitive mantle normalized trace element pattern for the average composition of shield and post erosional stages are similar to one another, although with differences in the Nb, Ta, and Sr enrichment and Rb, Pb depletions relative to neighbouring elements (Fig. 3). All studied basalts have fractionated heavy rare earth elements, with an average Gd/Yb ratio of 4.14 ± 0.3 in shield stage and 4.58 ± 0.07 in post-erosional lavas (Fig. 4). A Student's *t*-test returns a probability of 4×10^{-5} that the Gd/Yb ratios of post-erosional lavas are part of the shield stage lava population, demonstrating a significant difference. The general magnitude of the Gd/Yb ratios suggest that melting of plume material occurred in the garnet stability field. The difference between Gd/Yb of the two lava populations also suggests that either the post-erosional source contained more garnet than the shield-stage source or that the degree of melting in post-erosional lavas was generally lower than most shield-stage lavas (Fig. 4).

Similarly to trace element compositions, concentrations of first-row transition elements like Mn, Fe, Co, Ni, Zn can shed some light on the mantle source mineralogy. Melts of pyroxenites or eclogites would be expected to produce melts with higher Zn/Fe and lower Ni/Co and Co/Fe compared to peridotite partial melts (Humayun et al., 2004; Le Roux et al., 2010, 2011; Davis et al., 2013; Lang and Lambart, 2022). This is because the partitioning behaviours of these elements differ in pyroxenite/eclogite-vs peridotite-derived melts due to strong partitioning in clinopyroxene and garnet compared to orthopyroxene and olivine. Shield and post-erosional stage lavas have average Ni/Co of 5.7 and 3.5, respectively, (Co/Fe)×10 000 of 5.9 and 5.3, respectively, and (Zn/Fe)×10 000 of 11.7 and 11.1 (Fig. 5). These Ni/Co and (Co/Fe)×10 000 values are lower than those for melts generated from peridotite sources ($\gtrsim$6 and $\gtrsim$8, respectively; Le Roux et al., 2011), and (Zn/Fe)×10 000 slightly higher than melts generated from peridotite sources (∼8–10; Le Roux et al., 2010, 2011). This suggests that the sources of both stages of volcanism were variably enriched in clinopyroxene and garnet relative to the depleted mantle. The particularly low Ni/Co of post-erosional stage lavas (3.5) may indicate an even higher proportion of clinopyroxene/garnet in their source, consistent with a higher proportion of AOC.

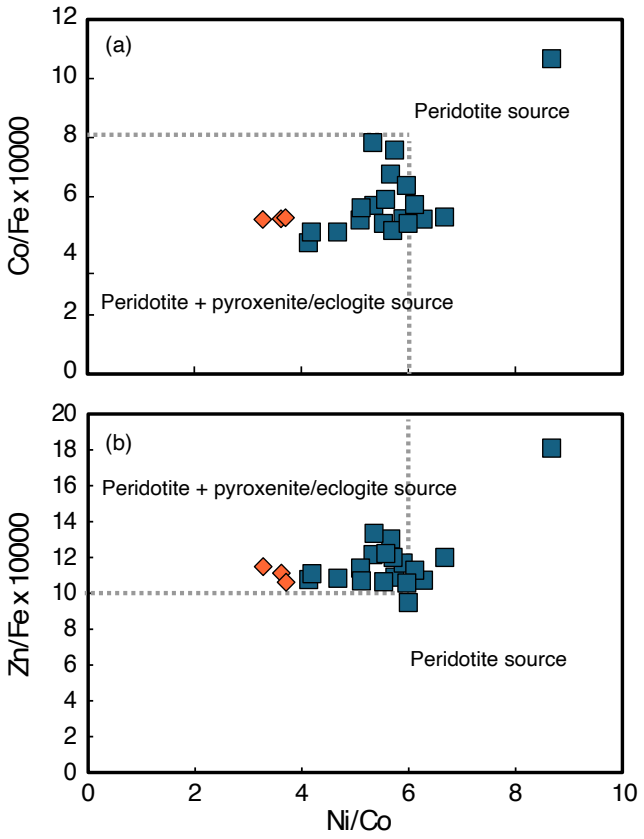

Figure 5. (Co/Fe)×10 000 (a) and (Zn/Fe)×10 000 (b) vs Ni/Co for basalts from Taha'a. The majority of samples appear to have been produced by melting of a peridotite source variably enriched in pyroxenite/eclogite (Le Roux et al., 2011). Symbols as in Figure 2. The vertical and horizontal lines mark the border of the field of partial melting of a primitive mantle-like peridotite source.

3.2 Effects from weathering, degassing and crustal assimilation on Tl isotopes

Before interpreting the Tl content and isotope compositions (see Table 4) in the context of a primary mantle source, it is important to first consider other processes that may have contributed to the observed variations. The main processes that could affect thallium isotope compositions

Table 1. Major element concentrations of Taha'a samples. Concentrations in wt.%.

Sample	SiO_2	Al_2O_3	TiO_2	MnO	Fe_2O_3	CaO	MgO	K_2O	Na_2O	P_2O_5
TAA-B-7	47.0	12.3	3.3	0.17	12.3	9.6	10.1	2.4	2.2	0.49
TAA-B-8	47.0	12.7	3.5	0.18	13.0	8.5	9.7	2.3	2.6	0.5
TAA-B-9	46.9	12.6	3.5	0.18	13.1	8.3	10.1	2.3	2.5	0.51
TAA-B-10	48.2	12.9	3.6	0.17	12.5	8.6	9.0	2.1	2.4	0.48
TAA-B-21	46.9	12.4	3.0	0.16	12.9	8.8	11.0	2.0	2.4	0.45
TAA-B-24	45.2	12.5	3.7	0.17	13.4	9.9	10.2	1.3	3.1	0.51
TAA-B-26	47.2	12.3	3.6	0.15	12.0	10.0	9.8	1.1	3.3	0.54
TAA-B-30	46.7	12.4	3.5	0.17	13.0	8.9	10.6	1.2	3.1	0.55
TAA-B-37	50.0	12.5	2.9	0.14	12.4	7.9	9.8	1.7	2.3	0.41
TAA-B-41	45.1	10.7	3.8	0.17	13.9	10.0	12.2	0.9	2.6	0.47
TAA-B-48	47.3	10.9	3.9	0.16	13.5	10.0	10.4	1.0	2.3	0.46
TAA-B-50	45.9	12.6	3.5	0.17	13.4	9.3	10.8	1.7	2.2	0.47
TAA-B-55	49.2	12.8	2.9	0.16	12.4	9.0	9.2	1.6	2.4	0.35
TAA-B-59	47.9	12.9	2.9	0.17	12.8	9.4	9.1	1.8	2.7	0.41
TAA-B-62	45.6	10.6	3.4	0.17	13.5	10.9	12.1	1.7	1.6	0.42
TAA-B-64	49.3	12.6	3.2	0.15	12.7	7.7	9.2	2.2	2.5	0.45
TAA-B-65	46.5	13.1	3.7	0.17	12.9	8.2	10.2	1.1	3.5	0.60
TAA-B-66	43.8	11.0	3.5	0.33	14.2	10.5	12.2	1.5	2.5	0.46
TAA-B-67	44.9	12.8	4.2	0.18	13.8	10.2	9.3	1.6	2.4	0.61
TAA-B-44†	43.0	13.5	4.1	0.2	13.4	11.4	7.7	2.0	4.2	0.64
TAA-B-45†	44.0	13.0	4.0	0.19	13.1	12.0	0.9	1.6	3.8	0.59
TAA-B-47†	41.8	11.8	3.7	0.21	14.5	12.3	10.4	0.8	3.9	0.63
BIR-1	47.1	15.3	1.0	0.18	11.8	13.2	9.5	0.03	1.9	0.03
BIR-1*	47.8	15.5	1.0	0.17	11.4	13.3	9.7	0.03	1.8	0.03

†: Post-erosional samples. All others are shield-stage samples.
BIR-1*: Recommended values from Jochum et al. (2016).

and concentrations are subaerial alteration, degassing, and assimilation of wall rock prior to eruption (Nielsen et al., 2016, 2021).

Although care was taken to select the freshest chips possible for analysis, it is unavoidable that Taha'a lavas were exposed to some amount of weathering in a tropical environment. To test whether secondary alteration minerals contributed to the Tl isotope composition of the samples, we leached five samples that cover the entire range of Tl isotope values encountered in our sample set (Table 4). Leached samples are all slightly enriched in the heavy Tl isotope relative to the unleached samples, although four of the five samples are within the long-term 2σ of ± 0.5 ε^{205}Tl-units. The one sample outside of analytical uncertainty has a Tl isotope composition only higher than the unleached samples by 1.2 ε^{205}Tl-units, and so only slightly outside the long-term 2σ of ± 0.5 ε^{205}Tl-units. Although these results suggest that minor amounts of material with low ε^{205}Tl were removed during leaching (possibly secondary clay minerals), these small differences are in stark contrast to submarine altered samples where differences between leached and unleached samples can be > 6 ε^{205}Tl-units (Kaare-Rasmussen et al., 2025). We, therefore, conclude that post-eruptive alteration effects on Tl isotopes in samples from Taha'a are limited. Given the large variability of ε^{205}Tl-values in the sample suite (−10.3 to +1.8) relative to the difference between leached and unleached samples (<1.2 ε^{205}Tl-units), potential contribution of Tl from secondary minerals are unlikely to affect interpretations.

Subaerial weathering can cause substantial loss of alkalis like Rb, Cs, or K (e.g., Schiano et al., 1993). Due to the geochemical similarity between Tl and the alkali metals, similar effects have been concluded for Tl (Nielsen et al., 2006a). As in previous studies (e.g., Blusztajn et al., 2018), we compare abundances of Tl and Cs to elements with similar compatibilities that are not sensitive to subaerial alteration like Ce and Th, respectively. Samples affected by severe alteration should be associated with anomalously high Ce/Tl and Th/Cs relative to other less altered samples. Lavas from OIBs generally exhibit Ce/Tl ≈ 1000–5000 and Th/Cs ≈ 5–30 (e.g., Kokfelt et al., 2006; Nielsen et al., 2006a; Willbold and Stracke, 2006; Nielsen et al., 2007; Brett et al., 2021). Although the Ce/Tl ratios of four samples (TAA-B-8, -21, -37 and -59) are within the range of other Taha'a samples and the typical values of OIBs (Fig. 6), their Th/Cs ratios vary between 50 and 113 (Fig. 6) and are much higher than all other samples in this study as well as observations in other OIBs (e.g., Kokfelt et al., 2006; Nielsen et al., 2006a; Willbold and Stracke, 2006; Nielsen et al., 2007; Blusztajn et al., 2018). The high Th/Cs is potentially indicative of alkali element loss due to weathering, although it is unclear how significantly Tl was affected based on sample Ce/Tl ratios. Weathering loss of Tl would likely not be associated with Tl isotope fractionation because weathering has been shown to cause negligible isotope fractionation (Nielsen et al., 2005). However, given the possibility of perturbation of the Tl budget in these four samples we conservatively exclude these from further discussion of the Tl isotopes.

Sample TAA-B-41 is characterized by the highest Tl content of 322 ng/g among all analyzed samples and a very low Ce/Tl = 250 and Th/Cs = 0.8, the latter being almost an order of magnitude lower than any other sample in this study. Given the light Tl isotope composition of

Table 2. Trace element concentrations of Taha'a samples. Concentrations in µg/g.

	TAA-B-7	TAA-B-8	TAA-B-9	TAA-B-10	TAA-B-21	TAA-B-24	TAA-B-26	TAA-B-30	TAA-B-37	TAA-B-41	TAA-B-48	TAA-B-50
Sc	21.8	16.4	21.0	21.5	21.4	22.2	20.6	20.9	16.1	23.8	10.3	20.4
V	222	218	221	223	187	244	223	213	177	251	255	224
Cr	478	369	486	386	458	381	339	421	577	590	592	420
Ni	361	349	399	160	278	249	257	269	307	320	332	265
Cu	40.8	27.6	27.3	26.6	31.2	33.7	34.2	32.5	26.2	44.5	41.1	49.9
Zn	105.0	118.6	100.1	94.2	104.8	106.9	112	99.9	103.9	104.3	106.9	100.3
Co	67.6	61.6	69.6	38.8	47.1	48.7	47.9	52.5	46.0	50.9	54.2	47.9
Cs	0.41	0.16	0.36	0.32	0.11	0.70	2.19	1.04	0.06	8.55	0.91	0.30
Rb	41.6	32.2	45.9	41.8	28.2	82.4	193	38.9	21.9	83.8	16.3	28.4
Ba	510	445	474	490	396	499	599	570	414	490	473	377
Th	7.86	8.21	8.75	8.87	7.26	7.11	9.82	9.75	6.91	7.25	5.96	5.38
U	1.28	1.36	1.45	1.42	1.17	1.17	1.82	1.60	0.89	1.16	1.28	0.96
Nb	45.9	47.5	47.7	48.5	35.2	44.2	55.7	52.6	35.7	45.2	45.9	36.9
Ta	3.46	3.53	3.58	3.64	2.72	3.27	3.92	3.80	2.75	3.47	3.51	2.77
La	38.2	40.7	41.5	42.4	39.1	37.3	48.8	46.1	37.2	38.7	39.9	31.9
Ce	91.8	93.2	94.9	96.7	89.6	86.0	113.6	108.8	79.1	90.6	92.4	76.7
Pb	5.25	5.96	4.82	5.15	5.25	4.70	6.59	6.37	5.16	7.30	4.63	3.96
Pr	10.39	10.38	10.56	10.74	10.58	9.87	12.94	12.33	9.6	10.44	10.91	8.95
Nd	44.7	44.5	45.3	45.9	45.9	44.2	54.8	52.1	43.0	45.9	48.0	40.2
Sr	583	499	519	528	549	668	728	683	507	604	610	544
Zr	317	308	306	309	308	287	399	376	275	286	287	255
Hf	8.18	7.97	8.02	8.16	8.19	7.67	9.78	9.49	7.35	7.78	7.71	6.67
Sm	8.75	8.87	9.14	9.24	9.17	9.37	10.13	9.75	9.28	9.46	9.75	8.67
Eu	2.58	2.62	2.68	2.73	2.68	2.83	2.87	2.78	2.77	2.80	2.92	2.67
Gd	7.42	7.71	7.97	8.06	7.97	8.17	8.14	7.86	8.35	8.04	8.35	7.62
Tb	1.11	1.17	1.20	1.22	1.19	1.21	1.18	1.14	1.24	1.18	1.21	1.14
Dy	5.28	5.58	5.74	5.83	5.67	5.57	5.49	5.35	5.95	5.48	5.63	5.39
Y	24.6	25.6	27.6	26.7	26.9	25.0	26.4	25.1	27.2	23.9	24.4	24.3
Ho	0.84	0.89	0.92	0.94	0.91	0.86	0.87	0.85	0.95	0.85	0.88	0.85
Er	2.51	2.64	2.73	2.74	2.68	2.44	2.61	2.52	2.78	2.42	2.50	2.47
Tm	0.31	0.33	0.34	0.34	0.33	0.29	0.32	0.31	0.34	0.29	0.30	0.30
Yb	1.90	1.99	2.05	2.08	1.99	1.73	1.96	1.91	2.05	1.71	1.79	1.83
Lu	0.27	0.29	0.29	0.30	0.29	0.24	0.29	0.28	0.29	0.24	0.25	0.26

	TAA-B-55	TAA-B-59	TAA-B-62	TAA-B-64	TAA-B-65	TAA-B-66	TAA-B-67	TAA-B-44†	TAA-B-45†	TAA-B-47†	BHVO-1	BHVO-1*
Sc	18.6	20.5	24.3	21.4	18.8	16.4	24.4	20.9	19.9	26.7	31.5	31.4
V	183	193	252	193	220	274	275	293	310	325	315	314
Cr	323	528	971	493	266	553	405	347	377	561	286	288
Ni	872	249	288	293	204	377	192	179	156	199	118	120
Cu	46.2	34.8	30.7	39.6	36.7	58.7	54.6	51.7	54.5	57.3	137.5	137.2
Zn	170.5	107.7	89.6	108.9	98.4	104.7	105.8	105	104.8	107.9	103.4	105.1
Co	100.5	43.5	48.1	52.7	43.6	63.1	45.8	49.5	47.7	53.8	44.0	44.9
Cs	0.23	0.19	0.74	0.41	0.71	0.47	0.43	1.25	0.96	1.98	0.1	0.1
Rb	30.2	26.8	34.4	45.7	101.7	22.7	30.1	34.2	28.9	18.7	9.4	9.5
Ba	325	391	567	546	619	424	425	685	684	748	131	134
Th	4.81	11.94	9.24	8.85	10.57	4.81	6.41	7.06	6.78	6.64	1.44	1.23
U	0.93	1.47	1.1	1.54	1.77	0.87	1.17	1.27	1.23	1.22	0.36	0.42
Nb	26.5	56.1	45.3	44.6	57.3	42.2	48.3	66.8	66.4	65.1	18.8	18.5
Ta	2.04	3.88	3.57	3.23	4.1	3.15	3.69	4.97	4.97	4.44	1.31	1.17
La	26.1	55.6	41.5	42	49.6	31.1	42.2	43.3	43.2	42.6	15.1	15.4
Ce	63.1	108.9	94.6	96.6	116.4	73.3	101.2	94.1	94.8	93.1	40.4	38.1
Pb	4.10	6.07	4.84	5.66	6.73	3.46	4.78	3.70	3.66	3.14	2.33	2.04
Pr	7.45	10.96	10.77	10.89	13.03	8.49	11.86	10.2	10.34	10.28	5.04	5.42
Nd	33.6	44.7	46.0	46.0	54.9	38.3	53.1	44.2	45.2	44.7	24.8	24.8
Sr	393	590	587	572	704	595	673	839	883	929	402	399
Zr	240	279	268	325	399	226	353	277	279	256	176	175
Hf	6.59	7.41	7.48	8.22	9.92	6.1	9.08	6.79	6.94	6.11	4.61	4.44
Sm	7.41	9.05	9.06	8.75	10.11	8.33	11.27	9.34	9.69	9.46	6.23	6.17
Eu	2.21	2.66	2.69	2.55	2.87	2.61	3.46	2.98	3.08	2.99	2.13	2.05
Gd	6.89	7.93	7.91	7.25	8.12	7.47	9.98	8.27	8.64	8.33	6.28	6.29
Tb	1.07	1.19	1.17	1.06	1.18	1.13	1.49	1.23	1.28	1.23	1.02	0.95
Dy	5.28	5.69	5.49	4.98	5.50	5.29	7.00	5.76	5.99	5.71	5.20	5.27
Y	24.9	26.3	24.7	23.8	25.9	23.0	31.6	25.6	25.9	26.5	26.1	26.2
Ho	0.86	0.91	0.87	0.80	0.88	0.82	1.11	0.90	0.92	0.88	0.87	0.98
Er	2.57	2.67	2.55	2.35	2.63	2.34	3.20	2.55	2.60	2.52	2.61	2.50
Tm	0.33	0.33	0.31	0.29	0.32	0.28	0.39	0.31	0.31	0.30	0.33	0.33
Yb	1.99	2.02	1.87	1.79	1.98	1.66	2.32	1.83	1.86	1.81	2.04	1.99
Lu	0.29	0.29	0.27	0.26	0.29	0.24	0.33	0.26	0.26	0.26	0.29	0.28

†: Post-erosional samples. All others are shield-stage samples.
BHVO-1*: Recommended values from Jochum et al. (2016).

Table 3. Sr, Nd and Pb isotopic compositions of Taha'a bulk basalts.

Sample	$^{87}Sr/^{86}Sr$	$^{143}Nd/^{144}Nd$	$^{206}Pb/^{204}Pb$	$^{207}Pb/^{204}Pb$	$^{208Pb}/^{204}Pb$
TAA-B-7	0.705 94	0.512 65	19.155	15.625	38.918
TAA-B-8	0.705 76	0.512 67	19.219	15.631	38.966
TAA-B-9	0.705 77	0.512 68	19.220	15.632	38.968
TAA-B-10	0.705 74	0.512 67	19.218	15.632	38.968
TAA-B-21	0.706 37	0.512 64	19.240	15.639	39.039
TAA-B-24	0.705 55	0.512 74	19.093	15.612	38.844
TAA-B-26	0.706 25	0.512 62	19.228	15.635	38.943
TAA-B-30	0.706 15	0.512 62	19.230	15.635	38.945
TAA-B-37	0.706 46	0.512 62	19.151	15.630	38.956
TAA-B-41	0.705 50	0.512 80	19.198	15.629	38.951
TAA-B-48	0.705 59	0.512 72	19.204	15.629	38.956
TAA-B-50	0.705 32	0.512 73	19.115	15.608	38.882
TAA-B-55	0.706 44	0.512 60	19.219	15.641	39.014
TAA-B-59	0.706 21	0.512 62	19.597	15.655	39.571
TAA-B-62	0.705 87	0.512 68	19.244	15.638	38.964
TAA-B-64	0.706 45	0.512 62	19.204	15.640	38.978
TAA-B-65	0.706 14	0.512 62	19.232	15.636	38.947
TAA-B-66	0.704 49	0.512 87	19.026	15.586	38.730
TAA-B-67	0.704 36	0.512 84	19.151	15.601	38.841
TAA-B-44†	0.703 69	0.512 99	18.734	15.527	38.429
TAA-B-45†	0.703 70	0.513 01	18.797	15.532	38.508
TAA-B-47†	0.703 78	0.512 97	18.797	15.532	38.508

†: Post-erosional samples. All other samples are from the shield stage.
The internal precision for Sr and Nd isotopic measurements is 8–20 ppm (2se) and 8–30 ppm (2se) respectively.
The $^{206}Pb/^{204}Pb$, $^{207}Pb/^{204}Pb$ and $^{208}Pb/^{204}Pb$ have internal precision (2se) of 100–300 ppm (2se).

Table 4. Thallium concentrations and isotope ratios of Taha'a samples.

Sample	Tl (ng/g)	ε^{205}Tl mean*	ε^{205}Tl	ε^{205}Tl dup.	ε^{205}Tl leach
TAA-B-7	91	−3.3	−3.3		
TAA-B-8	54	−2.2 [a]	−2.2		
TAA-B-9	37	0.5 [b]	0.5		
TAA-B-10	44	0.2 [b]	0.2		
TAA-B-21	49	−1.2 [a]	−1.2		
TAA-B-24	66	−0.7 [b]	−0.7		
TAA-B-26	121	−3.3	−3.3		
TAA-B-30	126	−3.2	−3.2		
TAA-B-37	39	−2.9 [a]	−2.9		
TAA-B-41	320	−10.2 [a]	−10.2		
TAA-B-48	96	−5.1	−5.5	−5.8	−3.9
TAA-B-50	29	−2.9	−2.9		
TAA-B-55	58	−1.7	−1.7		
TAA-B-59	62	1.8 [a]	1.4		2.2
TAA-B-62	52	−2.3	−2.3		
TAA-B-64	52	1.2 [b]	1.0		1.3
TAA-B-65	119	−2.4	−2.4		
TAA-B-66	66	−3.9	−3.9		
TAA-B-67	31	0.3 [b]	0.3		
TAA-B-44†	190	−10.3	−10.3	−11.0	−9.5
TAA-B-45†	130	−8.7	−9.5	−8.9	−7.8
TAA-B-47†	26	−4.6	−4.4	−4.9	

†: Post-erosional samples. All others are shield-stage samples.
*: Average thallium isotope ratios of samples including duplicates and leached samples.
[a]: ε^{205}Tl-values filtered for potential alteration.
[b]: ε^{205}Tl-values filtered for potential degassing.
Internal precision of ε^{205}Tl is between 0.1 and 0.3.

this sample ($\varepsilon^{205}Tl = -10.2$), we suspect contamination from secondary clay minerals rich in Tl and Cs. Although similar clay mineral contamination has only previously been observed for submarine samples (Nielsen et al., 2016), we believe it is safer to eliminate this sample from further discussion of Taha'a mantle source Tl isotope composition.

Thallium is a volatile metal and can experience kinetic isotope fractionation during magmatic degassing where the light isotope is enriched in the gas phase (e.g., Nielsen et al., 2021). Such processes produce degassed lavas with decreasing Tl content and heavy thallium isotope compositions developing with increasing degree of degassing

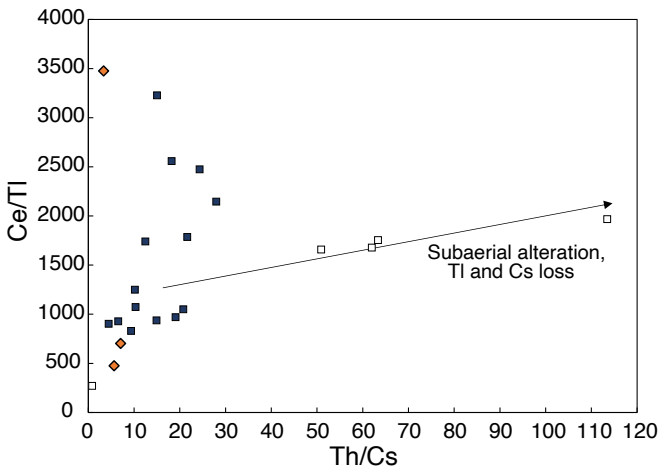

Figure 6. Ce/Tl plotted against Th/Cs. Four samples (TAA-B- 8, TAA-B-21, TAA-B-37 and TAA B-59) with very high Th/Cs > 50 and sample TAA-B-41 with extremely low Ce/Tl and Th/Cs were probably affected by subaerial alteration processes. They are shown as open squares. Symbols otherwise as in Figure 2.

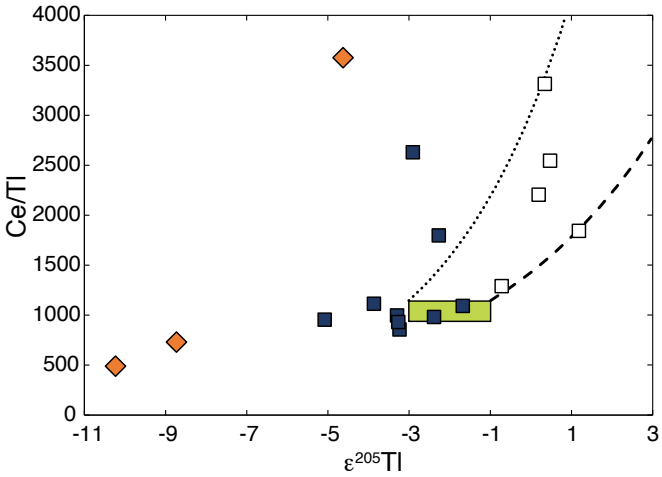

Figure 7. Thallium isotope compositions plotted against Ce/Tl ratios for lavas from Taha'a. Samples affected by post-eruption alteration not included in plot. Symbols as in Figure 2. Shown are also the two Tl loss models (Nielsen et al., 2021) with α_{net} = 0.99969 (dotted line) and α_{net} = 0.99955 (dashed line). Hypothetical undegassed starting point is characterized by Ce/Tl = 900–1150 and ε^{205}Tl = -2 ± 1. Five samples, which may have experienced degassing, are shown as open symbols.

(Nielsen et al., 2021). The net fractionation factor for natural basaltic lavas during degassing was shown to be α = 0.99955–0.99969 (Nielsen et al., 2021), which can be applied to groups of lavas from the same eruptive centre to determine if any lavas have experienced significant degassing. Examples from arc lavas and basalts from Azores (Nielsen et al., 2021; Shu et al., 2022b) clearly show that the processes responsible for Tl isotope fractionation in the laboratory experiments (Nielsen et al., 2021) must be very similar to those observed in natural lavas. Using the upper mantle Ce/Tl = 1150 (Nielsen et al., 2014) and ε^{205}Tl = −2.0 ± 1.0 (Nielsen et al., 2006a) as a hypothetical undegassed starting point, all samples with ε^{205}Tl > −1 fall within the area consistent with degassing (Fig. 7) based on the kinetic degassing model of Nielsen et al. (2021). Given that it cannot be known what the starting composition of undegassed lavas are, we can only infer that degassing may have contributed to the Tl abundance and isotope composition of these samples. We, therefore, do not further consider these samples in terms of mantle plume composition.

It is also notable that sample TAA-B-47 exhibits the highest Ce/Tl ratio of the entire data set, yet is characterized by ε^{205}Tl = −4.6 that is among the lowest values in our data set (Fig. 7). However, this sample belongs to the post-erosional group, which generally has the lowest Ce/Tl and ε^{205}Tl-values. While we cannot determine if TAA-B-47 was affected by degassing, we note that a degassing model using the other two post-erosional lavas as a starting point (Fig. 7) would go through the composition of TAA-B-47. We include TAA-B-47 for the remainder of the discussion but underscore the observation that post-erosional lavas exhibit substantially lower ε^{205}Tl-values than the shield stage lavas.

Finally, we also consider whether the observed light thallium isotope variations could be caused by crustal assimilation of AOC during magma transport. Although high-temperature-altered ocean crust has Tl isotope compositions similar to the upper mantle (ε^{205}Tl = −2.0 ± 1.0; Nielsen et al., 2006b), AOC has Tl isotope compositions that extend to much lower values (ε^{205}Tl = −2 to −15; Nielsen et al., 2006b).

In addition to having Tl isotope compositions extending to much lower values than the upper mantle (ε^{205}Tl = −2.0 ± 1.0; Nielsen et al., 2006b), AOC also carries distinct trace element contents and isotopic compositions. One of the most characteristic differences between AOC and basalts from Taha'a is their La/Nb ratio. In three sections of AOC, sites 504B (equatorial East-Pacific), 417/418 (West-Central Atlantic), and 801C (West Pacific), La/Nb varies from 1.18 to 1.97 (Staudigel et al., 1996; Bach et al., 2003; Kelley et al., 2003). These ratios are all higher than in Taha'a lavas (La/Nb = 0.65–0.98). If the variation in Taha'a lavas was caused by assimilation of 60 Ma old crust overlying Society Islands altered at low temperatures, increasing La/Nb would be associated with decreasing Tl isotopes ratios (Fig. 8). However, that is not the case (Fig. 8), meaning it is not possible to derive basalts from Taha'a through assimilation of AOC by mantle melts. Thus, Tl isotopic compositions of our samples do not record assimilated AOC.

Overall, 10 of the 22 samples analyzed in this study were filtered for potential secondary processes. The Tl isotope ratios of the remaining 12 lavas are hereafter interpreted to be representative of the mantle source from which they were derived. After removal of samples that may be affected by degassing and weathering, the overall Tl isotope variation observed in the Taha'a mantle source is ε^{205}Tl = −10.3

to −1.7. Results from Taha'a are in the range of ocean island basalts analyzed so far (Blusztajn et al., 2018; Brett et al., 2021; Williamson et al., 2021) with exception of two post erosional lavas which are characterized by a very light ε^{205}Tl −9.5, −7.8. In conjunction with radiogenic isotopes, two groups of lavas, shield and post-erosional, are clearly separated (Fig. 9).

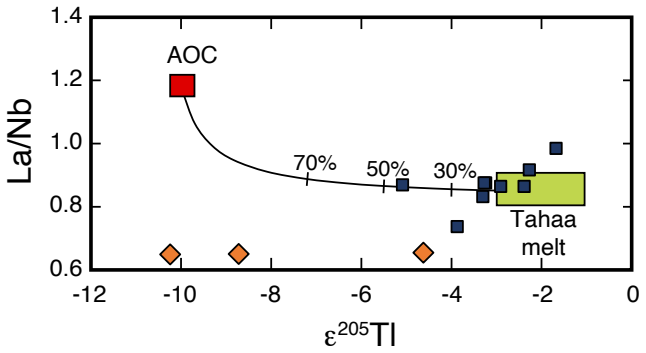

Figure 8. Thallium isotope composition of Taha'a lavas plotted versus La/Nb. Curve shows the relationship that is obtained for mixing between plume derived lavas with no Tl isotope anomaly (ε^{205}Tl = −2 and La/Nb = 0.85) and a hypothetical upper altered oceanic crust (AOC) based on data from ODP site 801C with La/Nb = 1.18 (Kelley et al., 2003). The Tl concentration and isotope composition of AOC is assumed to be 40 ng/g and ε^{205}Tl = −10. Samples potentially affected by weathering processes and degassing are not plotted. Symbols as in Figure 2.

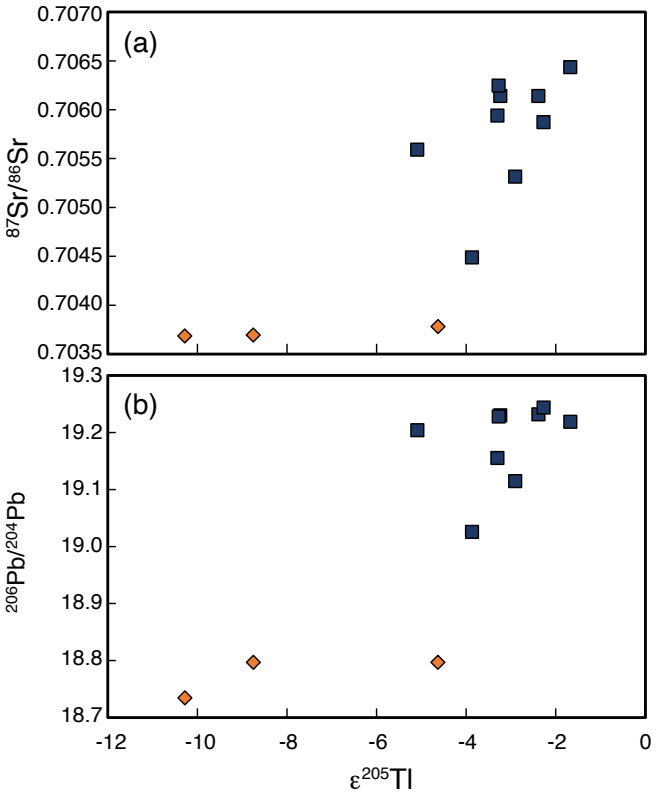

Figure 9. Tl isotopes plotted against (a) $^{87}Sr/^{86}Sr$ isotopes, (b) $^{206}Pb/^{204}Pb$ isotopes. Symbols as in Figure 2. Only samples unaffected by weathering and Tl degassing are plotted (see Section 3.2).

3.3 Origin of shield lavas

Most shield lavas in Taha'a record values within error of the upper mantle (ε^{205}Tl = −2 ± 1; Nielsen et al., 2006b), whereas post-erosional lavas all have values significantly lower than the average upper mantle (−4.6 to −10.3). Radiogenic isotopes also show an evolution of volcanism through time in Taha'a, in that shield stage and post-erosional stage volcanism are associated with different Tl, Sr, and Pb isotope compositions (Fig. 9). Additionally, trace element ratios sensitive to changes in the dominant mantle source component, such as Ce/Pb and Nb/Nb* (Nb/Nb* = $Nb_N/(Th_N \times La_N)^{1/2}$, where the subscript N indicates concentrations normalized to the primitive-mantle values of McDonough and Sun, 1995), are lower in shield stage lavas than in post erosional stage lavas (Figs 10 and 11).

The Tl isotope compositions of shield stage lavas, although mostly similar to the upper mantle, extend to values as low as ε^{205}Tl ≈ −5. This range in ε^{205}Tl-values, which co-varies with Ce/Pb and Nb/Nb* indicates that the plume source contained two components. The first is an isotopically enriched component dominated by mantle-like Tl isotopes, radiogenic Pb and Sr isotopes, and low Nb/Nb* and Ce/Pb ratios. These geochemical characteristics are consistent with a detrital sediment origin. The second component is characterized by low ε^{205}Tl, unradiogenic Sr and Pb isotopes, and higher Nb/Nb* and Ce/Pb ratios (Figs 9–11). Although the radiogenic isotope values of this second component are similar to the common mantle component FOZO (e.g., Weis et al., 2023), the remaining geochemical characteristics (in particular Tl isotopes) imply that AOC played a dominant role in its formation.

Previous literature has invoked the Society plume samples at Taha'a as an EM2 mantle plume (Fig. 2), most likely dominated by recycled sediments (e.g., White, 2010; Weis et al., 2023, and references therein). The enriched shield stage component bears all the characteristics of sedimentary material with radiogenic Pb and Sr isotopes, low Nb/U and Ce/Pb ratios (Hofmann et al., 1986; Hart, 1988; Plank, 2014). The mantle-like Tl isotope value of ε^{205}Tl ≈ −2 for this component is also identical to continental crust and terrigenous sediments (Nielsen et al., 2005, 2016) but distinct from modern deep-sea Mn-oxide-bearing pelagic sediments characterized by ε^{205}Tl > +2 (Rehkämper et al., 2004; Nielsen et al., 2016), suggesting that the EM2 component in Taha'a did not contain significant Mn oxides. Ancient sediments absent in Mn oxides could have been deposited in a largely anoxic deep ocean (Kaare-Rasmussen et al., 2025) or be similar to terrigenous sediments found on the modern continental shelves that also often are characterized by ε^{205}Tl ≈ −2 (Nielsen et al., 2016; Wang et al., 2022; Olesen et al., 2025). Therefore, ε^{205}Tl ≈ −2 in the EM2 endmember could be explained by either subducted terrigenous sediment or subducted ancient pelagic sediment deposited in an anoxic deep ocean.

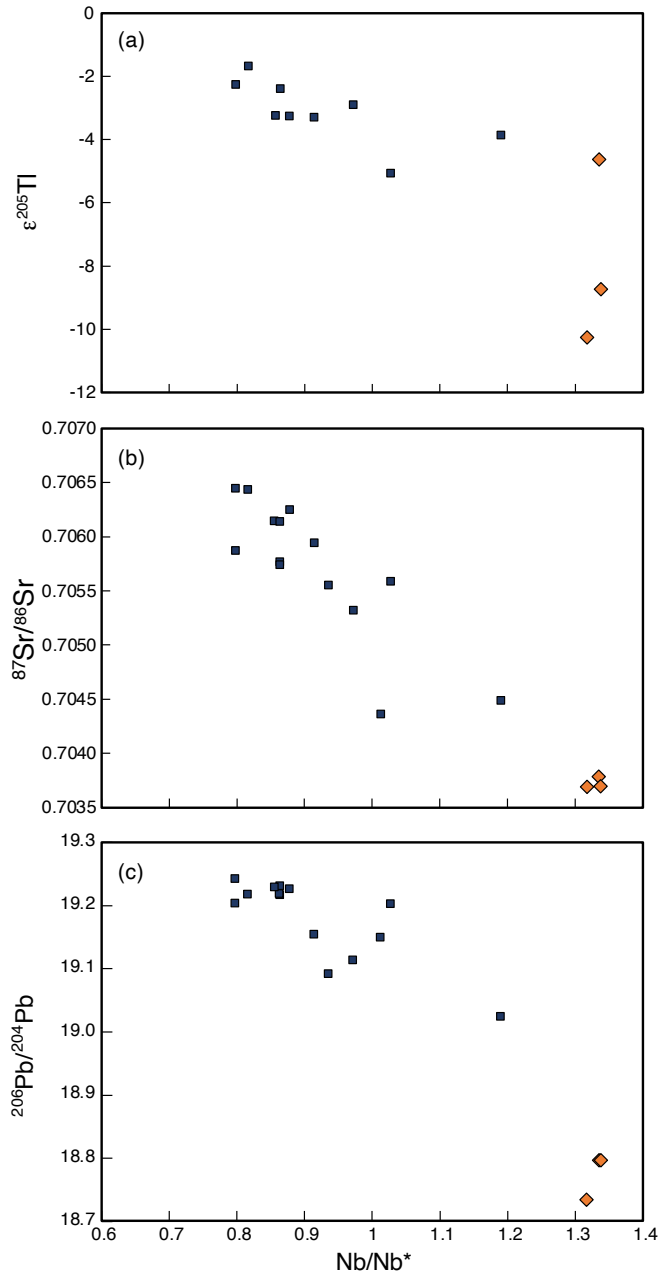

Figure 10. Niobium anomalies (Nb/Nb*) plotted against (a) Tl isotopes, (b) Sr isotopes, and (c) Pb isotopes. Symbols as in Figure 2. See text for definition of Nb/Nb*. In (a), (b), and (c), only samples unaffected by weathering and Tl degassing are plotted (see Section 3.2).

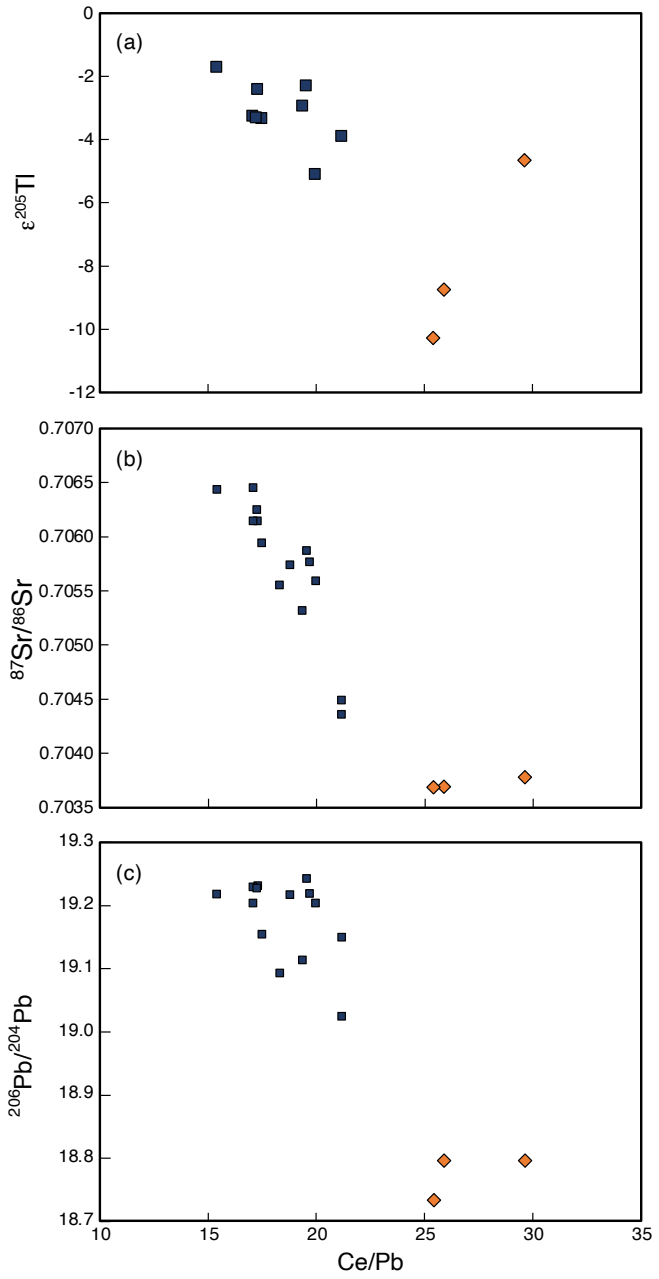

Figure 11. Ce/Pb plotted against (a) Tl isotopes, (b) Sr isotopes, and (c) Pb isotopes. Symbols as in Figure 2. In (a), (b), and (c), only samples unaffected by weathering and Tl degassing are plotted (see Section 3.2).

The isotopically depleted component in the shield stage lavas reveals Tl isotope compositions (ε^{205}Tl ≈ -5) within the range of AOC (ε^{205}Tl $= -2$ to -15; Nielsen et al., 2006b). Such low Tl isotope values are almost exclusively associated with AOC and only organic carbon rich shales have been shown to exhibit similar values (e.g., Ostrander et al., 2017). However, shales also contain large amounts of U (Andersen et al., 2017), which would result in high U/Th ratios for a recycled shale component. We observe no significant variation in U/Th among lavas from Taha'a (not plotted), effectively ruling shales out as a possible recycled component. The Sr and Pb isotope values and Ce/Pb and Nb/U ratios for this component do not correspond directly to those expected for ancient recycled AOC (Stracke et al., 2005; Bach et al., 2003; Chauvel et al., 1992), but the correlations between radiogenic isotopes, trace element ratios, and Tl isotopes strongly imply that subduction modified AOC best explains the second shield stage component.

3.4 Origin of post-erosional lavas

The results from several ODP and IODP cores show that the uppermost few hundred meters of AOC is the most Tl-enriched and exhibits the lowest Tl isotope values down to ε^{205}Tl ≈ -15 (Nielsen et al., 2017a). It is the only part of the subducted slab that has such low ε^{205}Tl-values. The

light Tl isotope values (ε^{205}Tl = −4.6 to −10.3) in Taha'a post-erosional lavas thus implies that post-erosional volcanism predominantly sampled a recycled AOC component. If the variation in Taha'a lavas was caused by assimilation of an old oceanic crust altered at low temperatures, increasing La/Nb would be associated with decreasing Tl isotopes ratios, which is not observed (Fig. 8). A similar range of Tl isotope compositions was observed in St. Helena (Blusztajn et al., 2018), which is considered the typical HIMU (high μ = ^{238}U/^{204}Pb) mantle endmember component thought to sample subducted AOC (see White, 2010, and references therein). Although Ce/Pb (∼27), Nb/U (∼53), Nb/Nb* (∼1.33) observed here for post-erosional Taha'a cannot directly be used to segregate mantle components (Weis et al., 2023; Harðardóttir and Jackson, 2025) their elevated ratios in the post-erosional lavas point towards values observed for HIMU-type OIBs (Chauvel et al., 1992; Cordier et al., 2021). While these ratios do not directly match AOC itself, it has been argued that subduction processing of AOC releases more Pb than U than Nb, resulting in these characteristic trace element signatures as well as the high time integrated μ-value (Bach et al., 2003; Chauvel et al., 1992; Stracke et al., 2005). These observations are consistent with an AOC origin of the post-erosional lavas in Taha'a.

The resemblance between the trace element and Tl isotopic characteristics of typical HIMU OIBs and the Taha'a post erosional component suggest that they share a similar origin. However, ^{206}Pb/^{204}Pb isotope ratios of post-erosional lavas are very unradiogenic in comparison to classical HIMU OIBs with ^{206}Pb/^{204}Pb > 21 (e.g., Stracke et al., 2005). The age of the recycled AOC will dictate the ^{206}Pb/^{204}Pb ratios of OIBs with relatively young recycled material obtaining substantially lower ^{206}Pb/^{204}Pb (Chauvel et al., 2024; Gurenko et al., 2006; Thirlwall, 1997) compared to the ∼2–2.4 Ga source age suggested for "typical" HIMU OIB such as St. Helena (e.g., Hanyu et al., 2014). Taken together, trace elements, radiogenic and Tl isotopes strongly imply that the post-erosional stage lavas were derived from a mantle source dominated by relatively young subduction modified AOC. Our data show that the isotopic difference between the "young HIMU" Taha'a source, and the typical HIMU source is most likely due to the difference in age of the recycled material.

It is important to highlight that Tl concentrations and isotope compositions in unsubducted AOC are very heterogeneous (Nielsen et al., 2006b, 2017b). Although subduction modification may lead to some amount of homogenization of the different slab components (Marschall and Schumacher, 2012; Nielsen and Marschall, 2017), it is likely that some Tl isotope heterogeneity persists in mantle sources sampling subducted AOC (e.g., Blusztajn et al., 2018). Thus, we anticipate that even the post-erosional stage at Taha'a would record substantial Tl isotope variation between AOC and MORB (Mid-ocean ridge basalts) if a larger sample set was investigated.

A mixture of recycled sediment and young AOC in the Society plume was previously proposed by Cordier et al. (2016, 2021) to explain observed variations in radiogenic isotopes and trace element characteristics of shield stage lavas from several Society Islands. However, the presence of a young AOC component in the Society plume has been debated (e.g., Saal et al., 2005). Other models include mixing sediments with ambient upper mantle (Duncan et al., 1994), or a common lower mantle component (White and Duncan, 1996; Saal et al., 1998, 2005). However, the low Tl isotope ratios in both Taha'a post-erosional and shield lavas provide strong evidence for young AOC in the Society mantle source. Previous authors have suggested that young (< 1.5 Ga) subducted AOC is common in many mantle plumes (Thirlwall, 1997; Stracke et al., 2005). Further analyses of Tl isotopes in other OIBs suggested to contain young AOC (e.g., Pitcairn, Canaries, Cape Verde, Comoros; Delavault et al., 2015; Cordier et al., 2021; Chauvel et al., 2024) can shed light on how common this component is in global OIBs.

3.5 Temporal evolution of Taha'a plume

The temporal changes in volcanism at Taha'a appear to be influenced by the nature of the dominant recycled components as the system evolved. Shield stage volcanism sampled AOC and detrital sediment material, which coexist in the mantle source and appear to contribute simultaneously in variable proportions, consistent with the conclusions of Cordier et al. (2016, 2021) for Society shield stage volcanism. In contrast, the post-erosional stage basalts (albeit based on only a few samples) show rather uniform radiogenic and trace element signatures. Although the Tl isotope compositions of the post-erosional lavas do exhibit substantial variation, it is possible that most of this variation is due to degassing (see discussion in Section 3.2).

The origin of the isotopically depleted component in several OIBs sampled by post-erosional lavas is a matter of debate. Depending on the geochemical characteristics of individual plumes, studies have argued for the source to be intrinsic to the plume (e.g., Fitton et al., 2003; Bizimis et al., 2013; DeFelice et al., 2019), entrained by the plume (e.g., Lassiter et al., 2000; Hofmann and Farnetani, 2013), or originating from melting of the lithosphere (Pilet et al., 2008; Béguelin et al., 2019). Because assimilation of oceanic lithosphere cannot explain our isotope data (Fig. 8) and entrainment of the ambient upper mantle (ε^{205}Tl = −2 ± 1; Nielsen et al., 2006a) is inconsistent with the light Tl isotope compositions, we suggest that the AOC component sampled by post-erosional is inherent to the Taha'a plume. Therefore, the plume responsible for Taha'a volcanism intrinsically contains mixed sediments and AOC components that may have melted separately during the shield stage. The pyroxenitic/eclogitic components of both shield and post-erosional samples (Fig. 5) are consistent with a plume geometry model where fertile, enriched components are distributed within the peridotite host, and contributed disproportionally to partial melting compared to the more refractory plume matrix (e.g., Koppers et al., 2021; Weis et al., 2023).

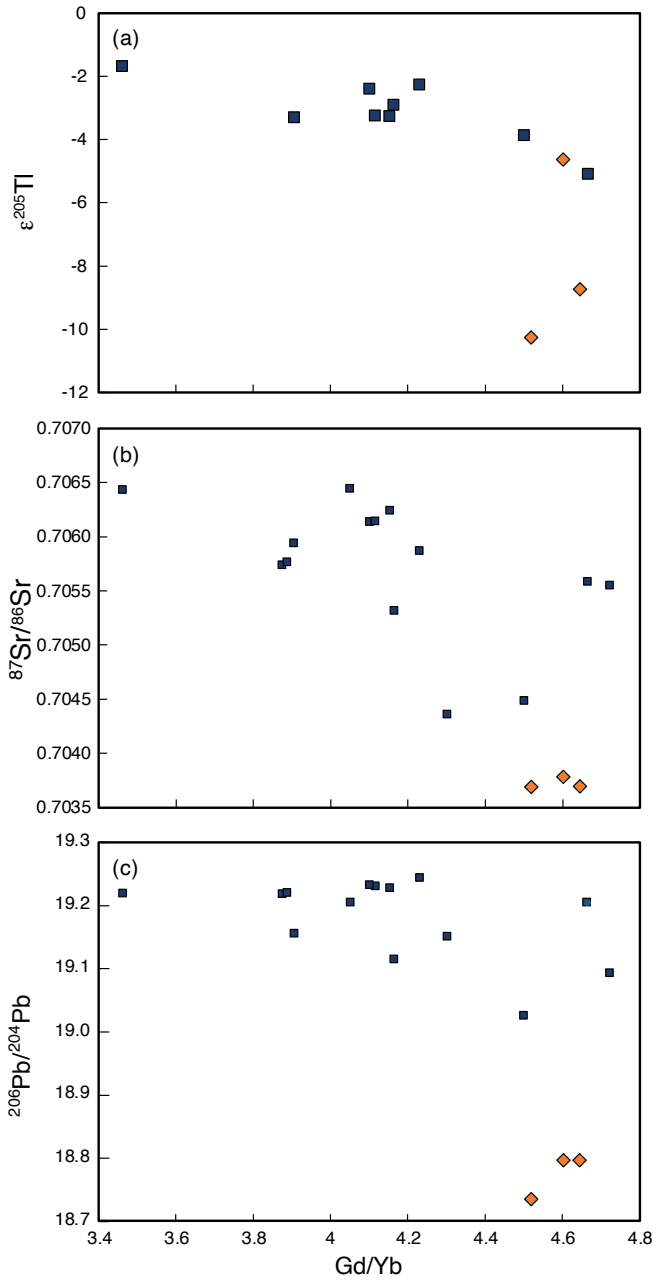

Figure 12. Gd/Yb plotted against (a) Tl isotopes, (b) Sr isotopes, and (c) Pb isotopes. Symbols as in Figure 2. In (a), (b), and (c), only samples unaffected by weathering and Tl degassing are plotted (see Section 3.2).

There are several potential reasons for the shift from mixed AOC-sediment components in shield stage volcanism to dominantly AOC component in the post-erosional component. The first is that the sediment component was exhausted during shield stage volcanism leaving only the AOC component to contribute to later post-erosional volcanism. However, White and Duncan (1996) showed an increase in the sediment component in late shield lavas. If the sediment component were exhausted during shield volcanism, the chemical signature of the late shield lavas would be expected to show an increase in the AOC component, not the sediment component. This suggests that exhaustion of the sediment component is unlikely to be responsible for the chemical shift between shield and post erosional stages.

An additional possibility is heterogenous distribution of components in the Society plume. Studies of the spatial relationships of multiple components within mantle plumes have shown that stretching of components within a plume during ascent will preserve their spatial relationships instead of mixing them chaotically (e.g., Abouchami et al., 2005; Farnetani et al., 2012, 2018; Jackson et al., 2014), sometimes resulting in double-track volcanic chains (Koppers et al., 2021, and references therein). Payne et al. (2013) suggested that the Society plume has bilateral chemical zonation, although such a conclusion has been disputed (Cordier et al., 2016). The possible chemical zonation in the Society plume means that change in plume components sampled by volcanism could result from local variations in the proportion of those components in the region of the plume contributing to volcanism on Taha'a during shield volcanism (3.4–2.6 Ma) and post-erosional volcanism (1.4–1.1 Ma). Assuming a stationary plume and a Pacific plate velocity of ~11 cm/year (Gripp and Gordon, 1990), Taha'a would have moved ~132 km relative to the plume axis during the ~1.2 Ma between the end of shield volcanism and the beginning of post-erosional volcanism. This distance is significantly larger than the diameter of the Society plume (several 10s of km; Uto et al., 2007). Although plumes are not perfectly stationary (e.g., Koppers et al., 2021, and references therein), the potential for Taha'a to have travelled such a large distance relative to the plume means a change in the relative proportion of components in the plume source sampled by different stages of volcanism is plausible.

Another possible explanation for the temporal shift on Taha'a is gravitational separation of components within the plume. It is notable that Tl, Sr, and Pb isotope ratios broadly correlate with Gd/Yb ratios (Fig. 12), which is indicative of the modal abundance of garnet in the source region (Fig. 4). In this case the correlations between Gd/Yb and isotope ratios (Fig. 12) suggest that the recycled AOC source is more enriched in garnet than the terrigenous sediment source apparent in many of the shield stage lavas. This observation is consistent with AOC being composed of more mafic material than terrigenous sediment, which produces larger modal abundances of garnet at high pressure than sediments (Poli and Schmidt, 2002). Given the high density of garnet, we speculate that the higher modal proportion of garnet in the AOC-dominated source could have caused a gravitational separation of the two components, slowing the upwelling of the denser AOC component and leading to the post-erosional stage sampling almost exclusively the AOC-dominated portion of the plume with entrainment of ambient upper mantle material.

4 Conclusions

There is strong evidence for systematic variation of the Tl isotope composition of Taha'a lavas through time. The shield stage lavas have more radiogenic Sr isotope values,

negative Nb anomalies, low Ce/Pb, and variable Tl isotopic compositions with $\varepsilon^{205}Tl = -5.1$ to -1.7. In comparison young, post-erosional lavas are characterized by unradiogenic Sr isotopes, positive Nb anomalies, low $^{206}Pb/^{204}Pb$, and Tl isotope values as low as $\varepsilon^{205}Tl = -10.3$. The systematic differences in Tl isotopic composition between shield and post-erosional stage volcanism in Taha'a in conjunction with radiogenic isotopes and trace element ratios indicative of source composition like Ce/Pb and Nb/Nb* reflects changes in compositional sources and their mixing proportions. The main shield building stage consists of both terrigenous sediment and AOC components, whereas AOC is predominantly present in the late post-erosional stage. The unradiogenic $^{206}Pb/^{204}Pb$ ratios of the post-erosional lavas implicate this portion of the plume as a "young HIMU" reservoir that contained subducted AOC that has not aged to the same extent as subducted AOC sampled at true HIMU localities like St. Helena. The Tl isotope data together with other geochemical tracers show that the EM2 mantle component manifested in the shield stage volcanism in Taha'a consists of continentally-derived sediment material plus variable amounts of AOC in the Society plume. Finally, correlations of Tl, Sr, Pb isotopes with Gd/Yb ratios suggest that the garnet abundance in the AOC-dominated part of the Taha'a plume was higher than the source containing terrigenous sediment. This conclusion is consistent with relative modal abundances of metamorphosed basaltic and sedimentary slab compositions (Poli and Schmidt, 2002). The higher garnet abundance in the younger post-erosional lavas could, therefore, be related to gravitational separation of the two plume components.

Acknowledgements

This study was funded by NSF grant EAR-1119373 to SGN. We are very grateful to editor Ananya Mallik and reviewers Nicole Williamson and Julie Prytulak whose comments and suggestions improved our manuscript.

Data, code, and outputs availability

All data acquired for this study are accessible in Blusztajn et al. (2026): https://doi.org/10.60520/IEDA/114421. Main text figures and tables are available for download in the online version of this article.

Competing interests

The authors declare that they have no known competing financial interests or personal relationships that could have appeared to influence the work reported in this paper.

Licence agreement

References

Abouchami W, Galer S, Koschinsky A (1999). Pb and Nd isotopes in NE Atlantic Fe–Mn crusts: Proxies for trace metal paleosources and paleocean circulation. *Geochimica et Cosmochimica Acta* 63(10): 1489–1505. doi:10.1016/s0016-7037(99)00068-x

Abouchami W, Hofmann AW, Galer SJG, Frey FA, Eisele J, Feigenson M (2005). Lead isotopes reveal bilateral asymmetry and vertical continuity in the Hawaiian mantle plume. *Nature* 434(7035): 851–856. doi:10.1038/nature03402

Andersen MB, Stirling CH, Weyer S (2017). Uranium Isotope Fractionation. *Reviews in Mineralogy and Geochemistry* 82(1): 799–850. doi:10.2138/rmg.2017.82.19

Bach W, Peucker-Ehrenbrink B, Hart SR, Blusztajn JS (2003). Geochemistry of hydrothermally altered oceanic crust: DSDP/ODP Hole 504B – Implications for seawater-crust exchange budgets and Sr- and Pb-isotopic evolution of the mantle. *Geochemistry, Geophysics, Geosystems* 4(3). doi:10.1029/2002gc000419

Binard N, Maury R, Guille G, Talandier J, Gillot P, Cotten J (1993). Mehetia Island, South Pacific: geology and petrology of the emerged part of the Society hot spot. *Journal of Volcanology and Geothermal Research* 55(3–4): 239–260. doi:10.1016/0377-0273(93)90040-x

Bizimis M, Salters VJM, Garcia MO, Norman MD (2013). The composition and distribution of the rejuvenated component across the Hawaiian plume: Hf-Nd-Sr-Pb isotope systematics of Kaula lavas and pyroxenite xenoliths. *Geochemistry, Geophysics, Geosystems* 14(10): 4458–4478. doi:10.1002/ggge.20250

Blusztajn J, Nielsen S, Le Roux V, Dunlea A, Segee-Wright G (2026). Major, trace elements content, radiogenic isotopes plus thallium isotopes in Taha'a (Society Island) plume v.2, Version 1.0. Interdisciplinary Earth Data Alliance (IEDA). doi:10.60520/IEDA/114421

Blusztajn J, Nielsen SG, Marschall HR, Shu Y, Ostrander CM, Hanyu T (2018). Thallium isotope systematics in volcanic rocks from St. Helena – Constraints on the origin of the HIMU reservoir. *Chemical Geology* 476: 292–301. doi:10.1016/j.chemgeo.2017.11.025

Brett E, Prytulak J, Rehkämper M, Hammond S, Chauvel C, Stracke A, Willbold M (2021). Thallium elemental and isotopic systematics in ocean island lavas. *Geochimica et Cosmochimica Acta* 301: 187–210. doi:10.1016/j.gca.2021.02.035

Béguelin P, Bizimis M, McIntosh EC, Cousens B, Clague DA (2019). Sources vs processes: Unraveling the compositional heterogeneity of rejuvenated-type Hawaiian magmas. *Earth and Planetary Science Letters* 514: 119–129. doi:10.1016/j.epsl.2019.03.011

Chauvel C, Hofmann AW, Vidal P (1992). HIMU-EM: The French Polynesian connection. *Earth and Planetary Science Letters* 110(1–4): 99–119. doi:10.1016/0012-821x(92)90042-t

Chauvel C, Inglis EC, Gutierrez P, Luu TH, Burckel P, Besson P (2024). Fani Maoré, a new "young HIMU" volcano with extreme geochemistry. *Earth and Planetary Science Letters* 626: 118529. doi:10.1016/j.epsl.2023.118529

Clague DA, Dalrymple GB (1987). The Hawaiian-Emperor volcanic chain, part I: Geological evolution. In Decker R (ed.) *Volcanism in Hawaii*, p. 5–54. Professional Paper 1350, US Geological Survey. doi:10.3133/pp1350

Cordier C, Chauvel C, Hémond C (2016). High-precision lead isotopes and stripy plumes: Revisiting the Society chain in French Polynesia. *Geochimica et Cosmochimica Acta* 189: 236–250. doi:10.1016/j.gca.2016.06.010

Cordier C, Delavault H, Chauvel C (2021). Geochemistry of the Society and Pitcairn-Gambier mantle plumes: What they share and do not share. *Geochimica et Cosmochimica Acta* 306: 362–384. doi:10.1016/j.gca.2021.04.014

Davis FA, Humayun M, Hirschmann MM, Cooper RS (2013). Experimentally determined mineral/melt partitioning of first-row transition elements (FRTE) during partial melting of peridotite at 3 GPa. *Geochimica et Cosmochimica Acta* 104: 232–260. doi:10.1016/j.gca.2012.11.009

De Muynck D, Huelga-Suarez G, Van Heghe L, Degryse P, Vanhaecke F (2009). Systematic evaluation of a strontium-specific extraction chromatographic resin for obtaining a purified Sr fraction with quantitative recovery from complex and Ca-rich matrices. *Journal of Analytical Atomic Spectrometry* 24(11): 1498. doi:10.1039/b908645e

DeFelice C, Mallick S, Saal AE, Huang S (2019). An isotopically depleted lower mantle component is intrinsic to the Hawaiian mantle plume. *Nature Geoscience* 12(6): 487–492. doi:10.1038/s41561-019-0348-0

Delavault H, Chauvel C, Sobolev A, Batanova V (2015). Combined petrological, geochemical and isotopic modeling of a plume source: Example of Gambier Island, Pitcairn chain. *Earth and Planetary Science Letters* 426: 23–35. doi:10.1016/j.epsl.2015.06.013

Duncan R, McDougall I (1976). Linear volcanism in French Polynesia. *Journal of Volcanology and Geothermal Research* 1(3): 197–227. doi:10.1016/0377-0273(76)90008-1

Duncan RA, Fisk MR, White WM, Nielsen RL (1994). Tahiti: Geochemical evolution of a French Polynesian Volcano. *Journal of Geophysical Research: Solid Earth* 99(B12): 24341–24357. doi:10.1029/94jb00991

Farnetani CG, Hofmann AW, Class C (2012). How double volcanic chains sample geochemical anomalies from the lowermost mantle. *Earth and Planetary Science Letters* 359–360: 240–247. doi:10.1016/j.epsl.2012.09.057

Farnetani CG, Hofmann AW, Duvernay T, Limare A (2018). Dynamics of rheological heterogeneities in mantle plumes. *Earth and Planetary Science Letters* 499: 74–82. doi:10.1016/j.epsl.2018.07.022

Fitton JG, Saunders AD, Kempton PD, Hardarson BS (2003). Does depleted mantle form an intrinsic part of the Iceland plume? *Geochemistry, Geophysics, Geosystems* 4(3). doi:10.1029/2002gc000424

Garcia MO, Swinnard L, Weis D, Greene AR, Tagami T, Sano H, Gandy CE (2010). Petrology, Geochemistry and Geochronology of Kaua'i Lavas over 4·5 Myr: Implications for the Origin of Rejuvenated Volcanism and the Evolution of the Hawaiian Plume. *Journal of Petrology* 51(7): 1507–1540. doi:10.1093/petrology/egq027

Geldmacher J, Hoernle K (2000). The 72 Ma geochemical evolution of the Madeira hotspot (eastern North Atlantic): recycling of Paleozoic ($\leq$500 Ma) oceanic lithosphere. *Earth and Planetary Science Letters* 183(1–2): 73–92. doi:10.1016/s0012-821x(00)00266-1

Gripp AE, Gordon RG (1990). Current plate velocities relative to the hotspots incorporating the NUVEL-1 global plate motion model. *Geophysical Research Letters* 17(8): 1109–1112. doi:10.1029/gl017i008p01109

Gurenko A, Hoernle K, Hauff F, Schmincke HU, Han D, Miura Y, Kaneoka I (2006). Major, trace element and Nd–Sr–Pb–O–He–Ar isotope signatures of shield stage lavas from the central and western Canary Islands: Insights into mantle and crustal processes. *Chemical Geology* 233(1–2): 75–112. doi:10.1016/j.chemgeo.2006.02.016

Hanyu T, Kawabata H, Tatsumi Y, Kimura JI, Hyodo H, Sato K, Miyazaki T, Chang Q, Hirahara Y, Takahashi T, Senda R, Nakai S (2014). Isotope evolution in the HIMU reservoir beneath St. Helena: Implications for the mantle recycling of U and Th. *Geochimica et Cosmochimica Acta* 143: 232–252. doi:10.1016/j.gca.2014.03.016

Harrison LN, Weis D, Garcia MO (2020). The multiple depleted mantle components in the Hawaiian-Emperor chain. *Chemical Geology* 532: 119324. doi:10.1016/j.chemgeo.2019.119324

Hart SR (1988). Heterogeneous mantle domains: signatures, genesis and mixing chronologies. *Earth and Planetary Science Letters* 90(3): 273–296. doi:10.1016/0012-821x(88)90131-8

Harðardóttir S, Jackson MG (2025). A new geochemical database for ocean island basalts: Inferring an OIB mantle source from unevenly sampled oceanic hotspots. *Chemical Geology* 672: 122505. doi:10.1016/j.chemgeo.2024.122505

Hoernle K, Schmincke HU (1993). The Petrology of the Tholeiites through Melilite Nephelinites on Gran Canaria, Canary Islands: Crystal Fractionation, Accumulation, and Depths of Melting. *Journal of Petrology* 34(3): 573–597. doi:10.1093/petrology/34.3.573

Hofmann A, Jochum K, Seufert M, White W (1986). Nb and Pb in oceanic basalts: new constraints on mantle evolution. *Earth and Planetary Science Letters* 79(1–2): 33–45. doi:10.1016/0012-821x(86)90038-5

Hofmann AW (1997). Mantle geochemistry: the message from oceanic volcanism. *Nature* 385(6613): 219–229. doi:10.1038/385219a0

Hofmann AW, Farnetani CG (2013). Two views of Hawaiian plume structure. *Geochemistry, Geophysics, Geosystems* 14(12): 5308–5322. doi:10.1002/2013gc004942

Humayun M, Qin L, Norman MD (2004). Geochemical Evidence for Excess Iron in the Mantle Beneath Hawaii. *Science* 306(5693): 91–94. doi:10.1126/science.1101050

Jackson MG, Hart SR, Konter JG, Kurz MD, Blusztajn J, Farley KA (2014). Helium and lead isotopes reveal the geochemical geometry of the Samoan plume. *Nature* 514(7522): 355–358. doi:10.1038/nature13794

Jackson MG, Hart SR, Koppers AAP, Staudigel H, Konter J, Blusztajn J, Kurz M, Russell JA (2007). The return of subducted continental crust in Samoan lavas. *Nature* 448(7154): 684–687. doi:10.1038/nature06048

Jochum KP, Weis U, Schwager B, Stoll B, Wilson SA, Haug GH, Andreae MO, Enzweiler J (2016). Reference values following ISO guidelines for frequently requested rock reference materials. *Geostandards and Geoanalytical Research* 40(3): 333–350. doi:10.1111/j.1751-908x.2015.00392.x

Kaare-Rasmussen J, Horton F, Ostrander C, Nielsen S (2025). Thallium isotope data suggest minimal recycled material within the proto-Iceland mantle plume source. *Chemical Geology* 685: 122798. doi:10.1016/j.chemgeo.2025.122798

Kelley KA, Plank T, Ludden J, Staudigel H (2003). Composition of altered oceanic crust at ODP Sites 801 and 1149. *Geochemistry, Geophysics, Geosystems* 4(6). doi:10.1029/2002gc000435

Kokfelt T, Hoernle K, Hauff F, Fiebig J, Werner R, Nberg D (2006). Combined trace element and Pb-Nd–Sr-O isotope evidence for recycled oceanic crust (upper and lower) in the Iceland mantle plume. *Journal of Petrology* 47(9): 1705–1749. doi:10.1093/petrology/egl025

Konter JG, Jackson MG (2012). Large volumes of rejuvenated volcanism in Samoa: Evidence supporting a tectonic influence on late-stage volcanism. *Geochemistry, Geophysics, Geosystems* 13(6). doi:10.1029/2011gc003974

Koppers AAP, Becker TW, Jackson MG, Konrad K, Müller RD, Romanowicz B, Steinberger B, Whittaker JM (2021). Mantle plumes and their role in Earth processes. *Nature Reviews Earth & Environment* 2(6): 382–401. doi:10.1038/s43017-021-00168-6

Krein SB, Behn MD, Grove TL (2020). Origins of Major Element, Trace Element, and Isotope Garnet Signatures in Mid-Ocean Ridge Basalts. *Journal of Geophysical Research: Solid Earth* 125(12): e2020JB019612. doi:10.1029/2020jb019612

Lang OI, Lambart S (2022). First-row transition elements in pyroxenites and peridotites: A promising tool for constraining mantle source mineralogy. *Chemical Geology* 612: 121137. doi:10.1016/j.chemgeo.2022.121137

Lassiter J, Hauri E, Reiners P, Garcia M (2000). Generation of Hawaiian post-erosional lavas by melting of a mixed lherzolite/pyroxenite source. *Earth and Planetary Science Letters* 178(3–4): 269–284. doi:10.1016/s0012-821x(00)00084-4

Le Roux V, Dasgupta R, Lee CT (2011). Mineralogical heterogeneities in the Earth's mantle: Constraints from Mn, Co, Ni and Zn partitioning during partial melting. *Earth and Planetary Science Letters* 307(3–4): 395–408. doi:10.1016/j.epsl.2011.05.014

Le Roux V, Lee CT, Turner S (2010). Zn/Fe systematics in mafic and ultramafic systems: Implications for detecting major element heterogeneities in the Earth's mantle. *Geochimica et Cosmochimica Acta* 74(9): 2779–2796. doi:10.1016/j.gca.2010.02.004

Marschall HR, Schumacher JC (2012). Arc magmas sourced from mélange diapirs in subduction zones. *Nature Geoscience* 5(12): 862–867. doi:10.1038/ngeo1634

McDonough W, Sun Ss (1995). The composition of the Earth. *Chemical Geology* 120(3–4): 223–253. doi:10.1016/0009-2541(94)00140-4

Nielsen SG, Marschall HR (2017). Geochemical evidence for mélange melting in global arcs. *Science Advances* 3(4). doi:10.1126/sciadv.1602402

Nielsen SG, Prytulak J, Blusztajn J, Shu Y, Auro M, Regelous M, Walker J (2017a). Thallium isotopes as tracers of recycled materials in subduction zones: Review and new data for lavas from Tonga-Kermadec and Central America. *Journal of Volcanology and Geothermal Research* 339: 23–40. doi:10.1016/j.jvolgeores.2017.04.024

Nielsen SG, Rehkämper M, Baker J, Halliday AN (2004). The precise and accurate determination of thallium isotope compositions and concentrations for water samples by MC-ICPMS. *Chemical Geology* 204(1–2): 109–124. doi:10.1016/j.chemgeo.2003.11.006

Nielsen SG, Rehkämper M, Brandon AD, Norman MD, Turner S, O'Reilly SY (2007). Thallium isotopes in Iceland and Azores lavas — Implications for the role of altered crust and mantle geochemistry. *Earth and Planetary Science Letters* 264(1–2): 332–345. doi:10.1016/j.epsl.2007.10.008

Nielsen SG, Rehkämper M, Norman MD, Halliday AN, Harrison D (2006a). Thallium isotopic evidence for ferromanganese sediments in the mantle source of Hawaiian basalts. *Nature* 439(7074): 314–317. doi:10.1038/nature04450

Nielsen SG, Rehkämper M, Porcelli D, Andersson P, Halliday AN, Swarzenski PW, Latkoczy C, Günther D (2005). Thallium isotope composition of the upper continental crust and rivers - An investigation of the continental sources of dissolved marine thallium. *Geochimica et Cosmochimica Acta* 69(8): 2007–2019. doi:10.1016/j.gca.2004.10.025

Nielsen SG, Rehkämper M, Prytulak J (2017b). Investigation and Application of Thallium Isotope Fractionation. *Reviews in Mineralogy and Geochemistry* 82(1): 759–798. doi:10.2138/rmg.2017.82.18

Nielsen SG, Rehkämper M, Teagle DA, Butterfield DA, Alt JC, Halliday AN (2006b). Hydrothermal fluid fluxes calculated from the isotopic mass balance of thallium in the ocean crust. *Earth and Planetary Science Letters* 251(1–2): 120–133. doi:10.1016/j.epsl.2006.09.002

Nielsen SG, Shimizu N, Lee CA, Behn MD (2014). Chalcophile behavior of thallium during MORB melting and implications for the sulfur content of the mantle. *Geochemistry, Geophysics, Geosystems* 15(12): 4905–4919. doi:10.1002/2014gc005536

Nielsen SG, Shu Y, Wood BJ, Blusztajn J, Auro M, Norris CA, Wörner G (2021). Thallium Isotope Fractionation During Magma Degassing: Evidence From Experiments and Kamchatka Arc Lavas. *Geochemistry, Geophysics, Geosystems* 22(5). doi:10.1029/2020gc009608

Nielsen SG, Yogodzinski G, Prytulak J, Plank T, Kay SM, Kay RW, Blusztajn J, Owens JD, Auro M, Kading T (2016). Tracking along-arc sediment inputs to the Aleutian arc using thallium isotopes. *Geochimica et Cosmochimica Acta* 181: 217–237. doi:10.1016/j.gca.2016.03.010

Noll P, Newsom H, Leeman W, Ryan J (1996). The role of hydrothermal fluids in the production of subduction zone magmas: Evidence from siderophile and chalcophile trace elements and boron. *Geochimica et Cosmochimica Acta* 60(4): 587–611. doi:10.1016/0016-7037(95)00405-x

Olesen KP, Nielsen SG, Ostrander CM, Udy N, Canfield DE (2025). Thallium cycling and boundary exchange in a continental margin basin. *Geochimica et Cosmochimica Acta* 399: 64–81. doi:10.1016/j.gca.2025.04.005

Ostrander CM, Owens JD, Nielsen SG (2017). Constraining the rate of oceanic deoxygenation leading up to a Cretaceous Oceanic Anoxic Event (OAE-2: 94 Ma). *Science Advances* 3(8). doi:10.1126/sciadv.1701020

Paul D, White WM, Blichert-Toft J (2005). Geochemistry of Mauritius and the origin of rejuvenescent volcanism on oceanic island volcanoes. *Geochemistry, Geophysics, Geosystems* 6(6). doi:10.1029/2004gc000883

Payne JA, Jackson MG, Hall PS (2013). Parallel volcano trends and geochemical asymmetry of the Society Islands hotspot track. *Geology* 41(1): 19–22. doi:10.1130/g33273.1

Pilet S, Baker MB, Stolper EM (2008). Metasomatized Lithosphere and the Origin of Alkaline Lavas. *Science* 320(5878): 916–919. doi:10.1126/science.1156563

Plank T (2014). 4.17 - The Chemical Composition of Subducting Sediments. In Holland HD, Turekian KK (eds.) *Treatise on Geochemistry (Second Edition)*, pp. 607–629. Elsevier, Oxford, second edition edn. doi:10.1016/B978-0-08-095975-7.00319-3

Poli S, Schmidt MW (2002). Petrology of Subducted Slabs. *Annual Review of Earth and Planetary Sciences* 30(1): 207–235. doi:10.1146/annurev.earth.30.091201.140550

Rehkämper M, Frank M, Hein J, Halliday A (2004). Cenozoic marine geochemistry of thallium deduced from isotopic studies of ferromanganese crusts and pelagic sediments. *Earth and Planetary Science Letters* 219(1–2): 77–91. doi:10.1016/s0012-821x(03)00703-9

Rehkämper M, Frank M, Hein J, Porcelli D, Halliday A, Ingri J, Liebetrau V (2002). Thallium isotope variations in seawater and hydrogenetic, diagenetic, and hydrothermal ferromanganese deposits. *Earth and Planetary Science Letters* 197(1–2): 65–81. doi:10.1016/s0012-821x(02)00462-4

Saal A, Hart S, Shimizu N, Hauri E, Layne G, Eiler J (2005). Pb isotopic variability in melt inclusions from the EMI–EMII–HIMU mantle end-members and the role of the oceanic lithosphere. *Earth and Planetary Science Letters* 240(3–4): 605–620. doi:10.1016/j.epsl.2005.10.002

Saal AE, Hart SR, Shimizu N, Hauri EH, Layne GD (1998). Pb Isotopic Variability in Melt Inclusions from Oceanic Island Basalts, Polynesia. *Science* 282(5393): 1481–1484. doi:10.1126/science.282.5393.1481

Scher HD, Delaney ML (2010). Breaking the glass ceiling for high resolution Nd isotope records in early Cenozoic paleoceanography. *Chemical Geology* 269(3–4): 329–338. doi:10.1016/j.chemgeo.2009.10.007

Schiano P, Dupré B, Lewin E (1993). Application of element concentration variability to the study of basalt alteration (Fangataufa atoll, French Polynesia). *Chemical Geology* 104(1–4): 99–124. doi:10.1016/0009-2541(93)90145-9

Shu Y, Nielsen SG, Le Roux V, Blusztajn J, Guo S, Huang F (2022a). Thallium isotope compositions of subduction-zone fluids: Insights from ultra-high pressure eclogites and veins in the Dabie terrane, eastern China. *Chemical Geology* 599: 120843. doi:10.1016/j.chemgeo.2022.120843

Shu Y, Nielsen SG, Le Roux V, Wörner G, Blusztajn J, Auro M (2022b). Sources of dehydration fluids underneath the Kamchatka arc. *Nature Communications* 13(1). doi:10.1038/s41467-022-32211-5

Shu Y, Nielsen SG, Marschall HR, John T, Blusztajn J, Auro M (2019). Closing the loop: Subducted eclogites match thallium isotope compositions of ocean island basalts. *Geochimica et Cosmochimica Acta* 250: 130–148. doi:10.1016/j.gca.2019.02.004

Shu Y, Nielsen SG, Zeng Z, Shinjo R, Blusztajn J, Wang X, Chen S (2017). Tracing subducted sediment inputs to the Ryukyu arc-Okinawa Trough system: Evidence from thallium isotopes. *Geochimica et Cosmochimica Acta* 217: 462–491. doi:10.1016/j.gca.2017.08.035

Staudigel H, Plank T, White B, Schmincke HU (1996). Geochemical Fluxes During Seafloor Alteration of the Basaltic Upper Oceanic Crust: DSDP Sites 417 and 418. In Bebout GE, Scholl DW, Kirby SH, Platt JP (eds.) *Subduction: Top to Bottom*, vol. 96, p. 19–38. American Geophysical Union. doi:10.1029/gm096p0019

Stracke A (2012). Earth's heterogeneous mantle: A product of convection-driven interaction between crust and mantle. *Chemical Geology* 330–331: 274–299. doi:10.1016/j.chemgeo.2012.08.007

Stracke A, Bizimis M, Salters VJM (2003). Recycling oceanic crust: Quantitative constraints. *Geochemistry, Geophysics, Geosystems* 4(3). doi:10.1029/2001gc000223

Stracke A, Hofmann AW, Hart SR (2005). FOZO, HIMU, and the rest of the mantle zoo. *Geochemistry, Geophysics, Geosystems* 6(5). doi:10.1029/2004gc000824

Thirlwall M (1997). Pb isotopic and elemental evidence for OIB derivation from young HIMU mantle. *Chemical Geology* 139(1–4): 51–74. doi:10.1016/s0009-2541(97)00033-8

Todt W, Cliff RA, Hanser A, Hofmann AW (1996). Evaluation of a 202Pb-205Pb double spike for high-precision lead isotope analysis. In Basu A, Hart SR (eds.) *Earth Processes: Reading the Isotopic Code*, vol. 95, p. 429–437. American Geophysical Union. doi:10.1029/gm095p0429

Uto K, Yamamoto Y, Sudo M, Uchiumi S, Ishizuka O, Kogiso T, Tsunakawa H (2007). New K-Ar ages of the Society Islands, French Polynesia, and implications for the Society hotspot feature. *Earth, Planets and Space* 59(7): 879–885. doi:10.1186/bf03352750

Wang Y, Lu W, Costa KM, Nielsen SG (2022). Beyond anoxia: Exploring sedimentary thallium isotopes in paleo-redox reconstructions from a new core top collection. *Geochimica et Cosmochimica Acta* 333: 347–361. doi:10.1016/j.gca.2022.07.022

Weis D, Harpp KS, Harrison LN, Boyet M, Chauvel C, Farnetani CG, Finlayson VA, Lee KKM, Parai R, Shahar A, Williamson NMB (2023). Earth's mantle composition revealed by mantle plumes. *Nature Reviews Earth & Environment* 4(9): 604–625. doi:10.1038/s43017-023-00467-0

Weis D, Kieffer B, Maerschalk C, Barling J, de Jong J, Williams GA, Hanano D, Pretorius W, Mattielli N, Scoates JS, Goolaerts A, Friedman RM, Mahoney JB (2006). High-precision isotopic characterization of USGS reference materials by TIMS and MC-ICP-MS. *Geochemistry, Geophysics, Geosystems* 7(8). doi:10.1029/2006gc001283

White WM (2010). Oceanic Island Basalts and Mantle Plumes: The Geochemical Perspective. *Annual Review of Earth and Planetary Sciences* 38(1): 133–160. doi:10.1146/annurev-earth-040809-152450

White WM, Duncan RA (1996). Geochemistry and Geochronology of the Society Islands: New Evidence for Deep Mantle Recycling. In Hart SR, Basu A (eds.) *Earth Processes: Reading the Isotopic Code*, vol. 95, p. 183–206. American Geophysical Union. doi:10.1029/gm095p0183

White WM, Hofmann AW (1982). Sr and Nd isotope geochemistry of oceanic basalts and mantle evolution. *Nature* 296(5860): 821–825. doi:10.1038/296821a0

Willbold M, Stracke A (2006). Trace element composition of mantle end-members: Implications for recycling of oceanic and upper and lower continental crust. *Geochemistry, Geophysics, Geosystems* 7(4). doi:10.1029/2005gc001005

Williamson NMB, Weis D, Prytulak J (2021). Thallium Isotopic Compositions in Hawaiian Lavas: Evidence for Recycled Materials on the Kea Side of the Hawaiian Mantle Plume. *Geochemistry, Geophysics, Geosystems* 22(9). doi:10.1029/2021gc009765

Zindler A, Hart S (1986). Chemical Geodynamics. *Annual Review of Earth and Planetary Sciences* 14(1): 493–571. doi:10.1146/annurev.ea.14.050186.002425